## ORIGINAL RESEARCH

Histamine Signaling Is Essential for Tissue Macrophage Differentiation and Suppression of Bacterial Overgrowth in the Stomach

Kwang H. Kim,[1,*] Jihwan Park,[2,*] Yejin Cho,[1] Soo Young Cho,[3] Buhyun Lee,[1] Haengdueng Jeong,[1] Yura Lee,[1] Ja-Woon Yi,[2] Yeseul Oh,[1] Jin-Jae Lee,[4] Timothy C. Wang,[5] Kyung-Min Lim,[6,§] and Ki Taek Nam[1,§]

[1]Severance Biomedical Science Institute, Brain Korea 21 PLUS Project for Medical Science, Yonsei University College of Medicine, Seoul, Republic of Korea; [2]School of Life Sciences, Gwangju Institute of Science and Technology, Gwangju, Republic of Korea; [3]Department of Molecular and Life Science, Hanyang University, Ansan, Republic of Korea; [4]Department of Life Science, Hallym University, Chuncheon, Republic of Korea; [5]Division of Digestive and Liver Diseases, Department of Medicine and Irving Cancer Center, Columbia University, New York, New York; and [6]College of Pharmacy, Ewha Womans University, Seoul, Republic of Korea
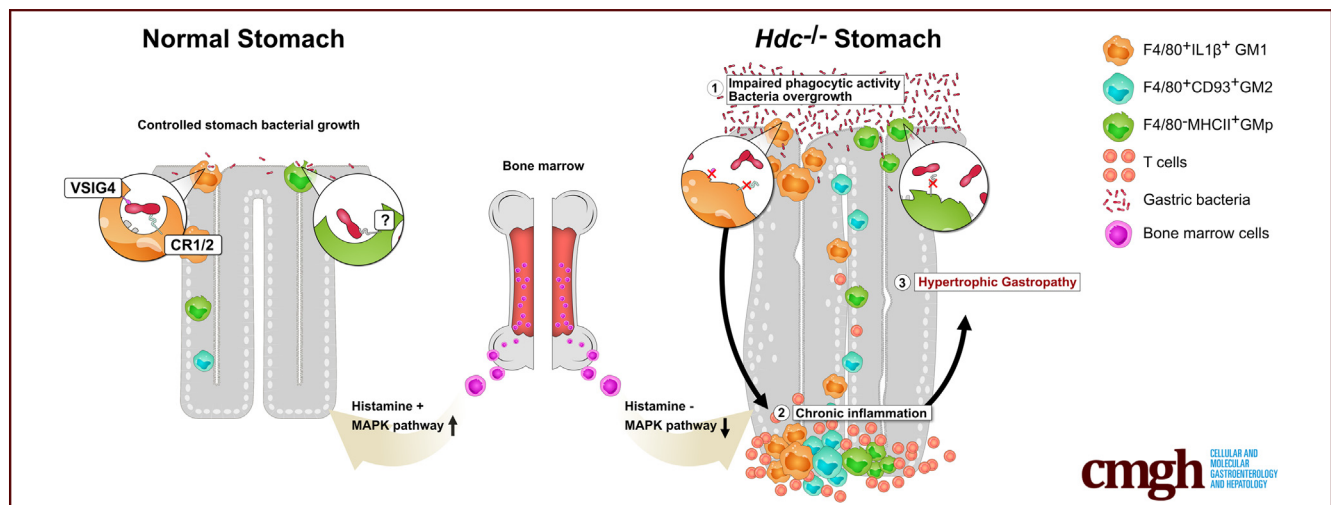
SUMMARY

We characterized stomach-specific macrophage populations and elucidated the importance of histamine in macrophage phagocytic activity for maintaining gastric homeostasis. Histamine deficiency results in hypertrophic gastropathy of the stomach, which is caused by abnormally differentiated macrophages.

BACKGROUND & AIMS: Histamine in the stomach traditionally is considered to regulate acid secretion but also has been reported to participate in macrophage differentiation, which plays an important role in tissue homeostasis. Therefore, this study aimed to uncover the precise role of histamine in mediating macrophage differentiation and in maintaining stomach homeostasis.

METHODS: Here, we expand on this role using histidine decarboxylase knockout ($Hdc^{-/-}$) mice with hypertrophic gastropathy. In-depth in vivo studies were performed in $Hdc^{-/-}$ mice, germ-free $Hdc^{-/-}$ mice, and bone-marrow–transplanted $Hdc^{-/-}$ mice. The stomach macrophage populations and function were characterized by flow cytometry. To identify stomach macrophages and find the new macrophage population, we performed single-cell RNA sequencing analysis on $Hdc^{+/+}$ and $Hdc^{-/-}$ stomach tissues.

RESULTS: Single-cell RNA sequencing and flow cytometry of the stomach cells of $Hdc^{-/-}$ mice showed alterations in the ratios of 3 distinct tissue macrophage populations (F4/80$^+$Il1b^{high}, F4/80$^+$CD93$^+$, and F4/80$^-$MHC class II^{high}CD74^{high}). Tissue macrophages of the stomachs of $Hdc^{-/-}$ mice showed impaired phagocytic activity, increasing the bacterial burden of the stomach and attenuating hypertrophic gastropathy in germ-free $Hdc^{-/-}$ mice. The transplantation of bone marrow cells of $Hdc^{+/+}$ mice to $Hdc^{-/-}$ mice recovered the normal differentiation of stomach macrophages and relieved the hypertrophic gastropathy of $Hdc^{-/-}$ mice.

CONCLUSIONS: This study showed the importance of histamine signaling in tissue macrophage differentiation and maintenance of gastric homeostasis through the suppression of bacterial

overgrowth in the stomach. *(Cell Mol Gastroenterol Hepatol 2023;15:213–236; https://doi.org/10.1016/j.jcmgh.2022.09.008)*

Keywords: Histidine Decarboxylase; Macrophage; Hypertrophic Gastropathy; Stomach.

<div style="border:1px solid black; text-align:center">

See editorial on page 277.

</div>

Histamine is a biogenic amine that orchestrates allergic responses and gastric acid production. Histamine also is involved closely in the regulation of immune responses. Endogenous histamine is produced via the conversion of L-histidine to histamine, which is catalyzed by histidine decarboxylase (HDC).[1] Mast cells generally are considered the major source of histamine.[2,3] Interestingly, in mast cell–deficient mice, even though the gastric histamine content is reduced by half, the intragastric pH, gastrin level, and gastric morphology are normal at 12 months of age. In contrast, the gastric mucosa of HDC-deficient mice shows mucosal hyperplasia in the oxyntic glandular base region with increased numbers of enterochromaffin-like cells and parietal cells,[4] and altered differentiation of the chief cell lineage,[5] suggesting the importance of non–mast-cell–originated histamine and histamine-mediated signaling in the maintenance of gastric homeostasis. However, the mechanism underlying the hypertrophic gastropathy of HDC-deficient mice is not fully explained.

Previous studies on HDC-deficient mice have shown that the histamine signal is important for the differentiation of myeloid cells. HDC deficiency led to the accumulation of $CD11b^+Ly6G^+$ immature myeloid cells,[6] and inhibited $CD8^+$ T-cell proliferation.[7] The histamine signal also promotes the differentiation of macrophages[8,9] and monocyte-derived dendritic cells.[10] Furthermore, the H_2-receptor–mediated signal was shown to be pivotal for the maintenance of myeloid-biased hematopoietic stem cells[11] and the differentiation of human monocyte-derived M1 macrophages,[12] suggesting a potential role of disrupted histamine signaling–mediated immunologic disorders in the development of hypertrophic gastropathy in HDC-deficient mice.

Macrophages play a pivotal role in the tissue repair and maintenance of tissue homeostasis by eliminating foreign antigens.[13,14] In the intestinal tract, tissue macrophages defend the intestinal barrier, a primary site of microorganism contact, through bacterial sampling at the luminal region, tissue remodeling, and elimination of penetrating bacteria. Furthermore, macrophages are important for the balance of the intestinal microbiome by suppressing bacterial overgrowth.[15] Of note, bacterial overgrowth in the stomach was found to induce chronic gastritis in mice.[16] However, the role of macrophages in hypertrophic gastropathy is not well understood. Moreover, tissue macrophages of the stomach have not yet been fully characterized, highlighting the urgent need for detailed studies on this topic.

Here, we show that histamine deficiency leads to impairment in tissue macrophage differentiation, which results in the emergence of a distinct immature macrophage population with disrupted phagocytic activity. Consistently, $Hdc^{-/-}$ mice showed uncontrolled bacterial overgrowth, which might have contributed to the development of hypertrophic gastropathy, at least in part. Collectively, this study highlights the importance of histamine signaling in the differentiation of tissue macrophages for the regulation of bacterial overgrowth and the maintenance of gastric homeostasis.

Results

Spontaneous Hypertrophic Gastropathy of Hdc$^{-/-}$ Mice

In line with previous reports,[4,5,17] the stomach fundic mucosal gland was remarkably thickened in $Hdc^{-/-}$ mice at 2 months after birth, and cyst structures were detected at the basal region in 5-month-old and 1-year-old $Hdc^{-/-}$ mice (Figure 1A and B). The size of H^+K^+–adenosine triphosphatase$^+$ parietal cells was decreased in $Hdc^{-/-}$ mice compared with those of $Hdc^{+/+}$ mice (Figure 1C). Ki67$^+$ proliferating cells normally localized in the isthmus region[18] were observed at increased numbers in the basal region of $Hdc^{-/-}$ mice (Figure 1D). Furthermore, inflammatory reactions were observed in the stomachs of 1-year-old $Hdc^{-/-}$ mice (Figure 1A) along with CD3$^+$ T-cell infiltration (Figure 1E). Immunofluorescence showed increased numbers of GSII (griffonia simplicifolia-II)$^+$GIF (gastric intrinsic factor)$^+$ cells,[19] a marker of spasmolytic polypeptide-expressing metaplasia, in the stomachs of 1-year-old $Hdc^{-/-}$ mice (12% vs 2%) (Figure 1F). CD44v9$^+$ cells also were detected in the stomachs of 1.5-year-old $Hdc^{-/-}$ mice (Figure 1G), which emerge in various types of metaplasia.[20]

To uncover the mechanism underlying the hypertrophic gastropathy of $Hdc^{-/-}$ mice, we performed a whole-transcript expression array using the stomach tissues of 1-year-old $Hdc^{+/+}$ and $Hdc^{-/-}$ mice. HALLMARK database analysis revealed the upregulation of inflammation- and tumorigenesis-related signaling pathways in the stomachs of 1-year-old $Hdc^{-/-}$ mice (Figure 2A). CIBERSORT analysis

Most current article

showed that the number of macrophages increased significantly in the stomachs of $Hdc^{-/-}$ mice (Figure 2B).[21] Quantitative polymerase chain reaction (qPCR) analysis showed a significant increase in the levels of proinflammatory genes that may be related with macrophage differentiation in the 1-year-old $Hdc^{-/-}$ mouse stomach compared with those in the stomachs of $Hdc^{+/+}$ mice (Figure 2C), suggesting a role of macrophages in hypertrophic gastropathy and chronic inflammation of the stomach in $Hdc^{-/-}$ mice.

Abnormally Differentiated Macrophages Accumulate in the Hdc$^{-/-}$ Mouse Stomach

To confirm the accumulation of macrophages in the stomachs of $Hdc^{-/-}$ mice, the histology of the stomach tissues was examined. A previous report showed that CD163$^+$F4/80$^+$ macrophages were increased significantly in the L635-induced gastric metaplasia model.[22] However, immunofluorescence staining failed to show any significant difference in CD163$^+$ macrophages in the stomachs of $Hdc^{+/+}$ mice compared with those of $Hdc^{-/-}$ mice (Figure 3A and B). Of note, CD163$^-$F4/80$^+$ macrophages massively infiltrated the stomachs of $Hdc^{-/-}$ mice (Figure 3A and C). Furthermore, Ki67$^+$F4/80$^+$ proliferating macrophages were detected in 5-month-old and 1-year-old $Hdc^{-/-}$ mouse stomachs (Figure 3D).

Blockade of the histamine signal can impair myeloid maturation.[6] We investigated the changes in the population of stomach tissue macrophages using flow cytometry. At 4 weeks, the number of CD11b$^+$F4/80$^+$ stomach macrophages was reduced in $Hdc^{-/-}$ mice, which was reversed at 1 year, likely owing to chronic inflammation. We further found that the number of CD11b$^+$F4/80$^-$ cells dramatically increased in the stomach tissue of the 1-year-old $Hdc^{-/-}$ mice (Figure 3E). Both the size (FSA) and granularity (SSC) of CD45$^+$CD11b$^+$F4/80$^+$ macrophages in the stomach were lower in 4-week-old $Hdc^{-/-}$ mice compared with those of $Hdc^{+/+}$ mice (Figure 3F), showing that the histamine deficiency may have affected the differentiation of stomach macrophages.

Histamine-Mediated Macrophage Differentiation Is Important for Phagocytic Function and Prevention of Stomach Dysbiosis

A previous study showed that histamine-H4-receptor–mediated signaling induces phagocytic activity in murine bone marrow–derived macrophages and RAW 264.7 cells.[23] Therefore, to confirm whether the phagocytic activity of stomach macrophages was altered in $Hdc^{-/-}$ mice, we performed a microbead-based phagocytosis assay. Stomach macrophages of $Hdc^{-/-}$ mice showed significantly impaired phagocytic activity compared with that of $Hdc^{+/+}$ mice; 1–6 beads containing CD11b$^+$ cells were decreased significantly in $Hdc^{-/-}$ mice relative to those of $Hdc^{+/+}$ mice, and most of the $Hdc^{-/-}$ CD11b$^+$ cells were negative for phycoerythrin (PE)-stained beads (Figure 4A and B). Because the phagocytotic activity of macrophages helps to control microbiota growth in the intestine,[24] we hypothesized that bacteria-suppressing activity might have been disrupted in the $Hdc^{-/-}$ stomach, which may have contributed to the

development of chronic inflammation. Anaerobic culture of stomach tissues on blood agar showed no differences in the microbial colony-forming unit (CFU) count between $Hdc^{+/+}$ and $Hdc^{-/-}$ mice at 4 weeks, whereas the CFU counts dramatically increased at in the stomachs of 1-year-old $Hdc^{-/-}$ mice compared with those of $Hdc^{+/+}$ mice (Figure 4C). Similar results were obtained with tissue cultures on aerobic Luria–Bertani agar or brain heart infusion agar (Figure 4D). 16s Ribosomal RNA sequencing to identify the composition of microbiota showed that histamine deficiency altered the stomach microbiome extensively (Figure 4E–H).

To explore whether the impaired gastric acid secretion by parietal cells, which rely on histamine signaling,[25] led to the increased bacterial growth in the stomachs of $Hdc^{-/-}$ mice, we eliminated the gut microbiota using an antibiotic cocktail and then the mice were orally administered the microbiota obtained from the stomach tissue of wild-type mice, with the stomach pH maintained in an acidic state for 30 days by supplying acidified drinking water[26] (Figure 5A). The cecum was enlarged in the antibiotic-treated group compared with that of the distilled water–treated group (Figure 5B). The total stomach bacterial CFU also decreased significantly in the antibiotic-treated $Hdc^{+/+}$ and $Hdc^{-/-}$ groups compared with those of the corresponding distilled water–treated controls (Figure 5C and D). After reconstitution of the microbiota with acidified water supplied for 30 days, the cecum returned to a normal size in all groups (Figure 5E), and the acidified water significantly lowered the stomach pH of the $Hdc^{-/-}$ group to reach the same level as that in $Hdc^{+/+}$ mice (Figure 5F). Importantly, increased bacterial growth in the $Hdc^{-/-}$ mouse stomach only partially was suppressed by the acidified water (Figure 5G), implying that reduced gastric acid secretion cannot fully explain the bacterial overgrowth and hypertrophic gastropathy of $Hdc^{-/-}$ mice.

To further investigate whether the stomach dysbiosis was the major cause of hypertrophic gastropathy, we generated germ-free (GF) $Hdc^{-/-}$ mice (Figure 6A and B). Of note, the stomach of 1-year-old GF-$Hdc^{-/-}$ mice did not show the abnormally increased fundic mucosal glands (Figure 6C), chronic inflammation, or mucosal tissue proliferation, as determined by significantly decreased CD3$^+$ cells (Figure 6D) and Ki67$^+$ proliferating cells (Figure 6E), respectively, compared with those of specific pathogen-free (SPF) $Hdc^{-/-}$ mice, indicating that impaired macrophage activity–mediated dysbiosis of the stomach is responsible for hypertrophic gastropathy.

Histamine-Mediated Mitogen-Activated Protein Kinase Signaling Is Required for Macrophage Differentiation at the Bone Marrow Stage

Histamine is important for macrophage differentiation during bone marrow (BM) stages.[11] The phagocytic activity of bone marrow–derived macrophages (BMDMs) of $Hdc^{-/-}$ mice was restored by histamine treatment, whereas that of peritoneal macrophages did not recover (Figure 7A and B). In addition, inhibition of histamine-activated pathways with 4-bromo-3-hydroxybenzoic acid[27] resulted in impairment of

the phagocytic function of BMDMs (Figure 7C). Further highlighting the importance of histamine signaling during macrophage differentiation from the BM, treatment of granulocyte-macrophage colony-stimulating factor (GMCSF), a cytokine driving macrophage differentiation, to the BM of $Hdc^{+/+}$ mice induced histamine production, whereas treatment of CSF-1 was less effective (Figure 7D). The activation of mitogen-activated protein kinase (MAPK)
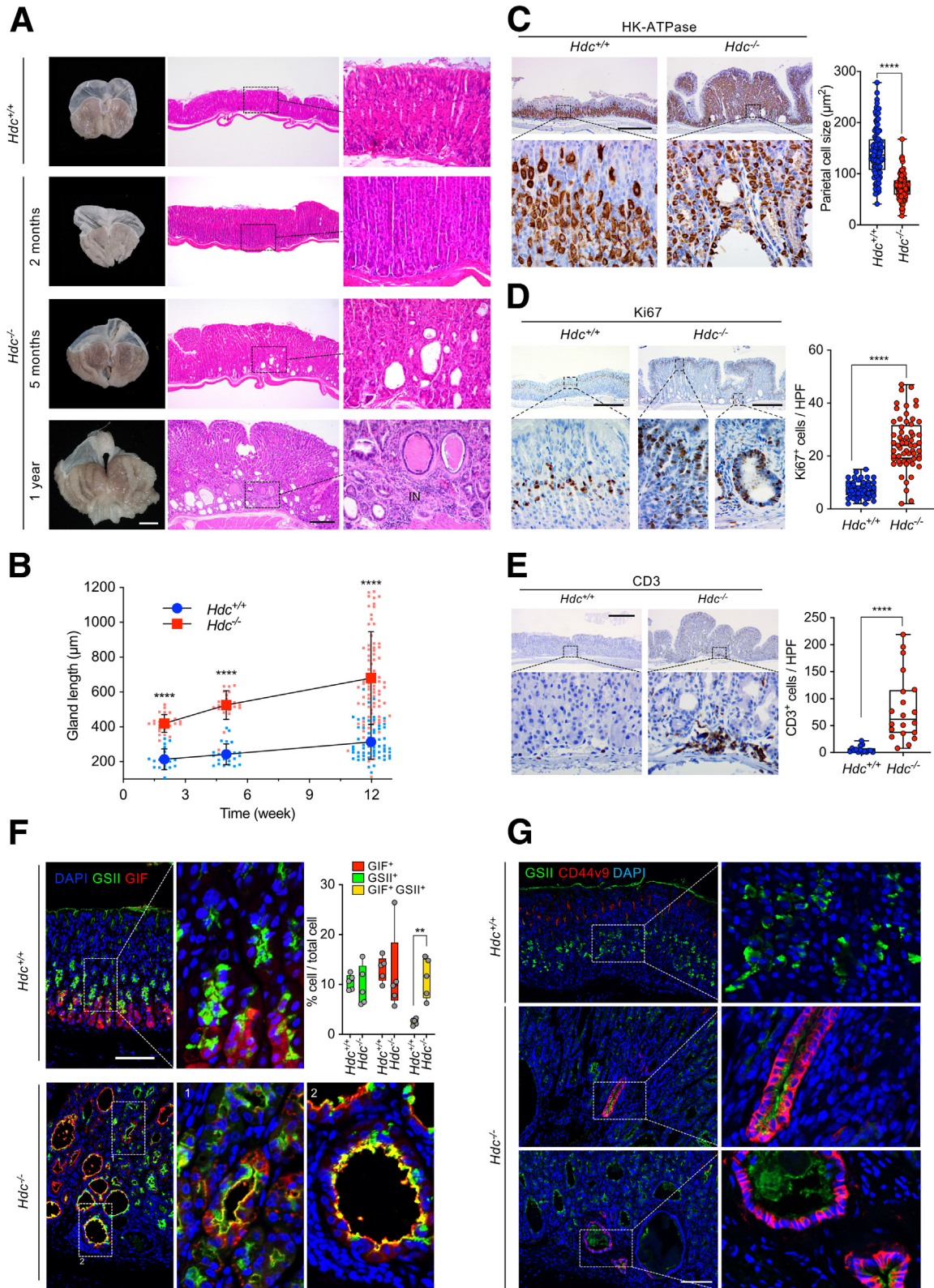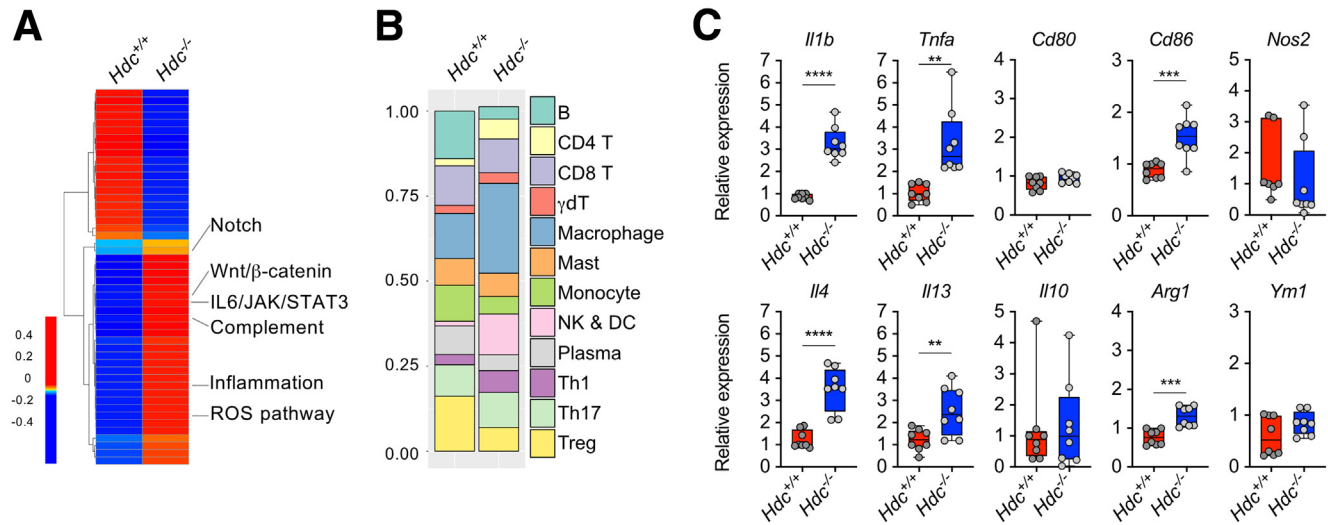
Figure 2. Macrophages are potentially associated with hypertrophic gastropathy. (*A*) Representative oligonucleotide microarray analysis of 1-year-old $Hdc^{+/+}$ and $Hdc^{-/-}$ mouse stomach tissues using the HALLMARK database with gene sets of interest highlighted. (*B*) CIBERSORT analysis of 1-year-old $Hdc^{+/+}$ and $Hdc^{-/-}$ mouse stomach tissues. (*C*) Expression of *Il1b*, *Tnfa*, *Cd80*, *CD86*, *Nos2*, *Il4*, *Il13*, *Il10*, *Arg1*, and *Ym1* in 1-year-old $Hdc^{+/+}$ and $Hdc^{-/-}$ mouse stomach tissues (n = 8 mice). Data are means ± SD. **$P < .01$, ***$P < .001$. JAK, janus kinase; ROS, reactive oxygen species; STAT3, signal transducer and activator of transcription 3.

signaling is important for BM macrophage development.[28] We therefore analyzed whether histamine is required for BM macrophage differentiation through activation of the MAPK pathway. Western blot was performed on BM cells from 2-month-old $Hdc^{+/+}$ and $Hdc^{-/-}$ mice with anti–phospho-extracellular-signal-regulated kinase (ERK), p38, and c-Jun N-terminal kinase (JNK) antibodies. The results showed that the phosphorylation of MAPK signaling molecules was impaired significantly in $Hdc^{-/-}$ BM cells (Figure 7E). However, we could not detect the phospho-ERK+ stomach macrophages in either $Hdc^{+/+}$ or $Hdc^{-/-}$ mice (Figure 7F). These data indicated that histamine is required for macrophage development via the MAPK signaling pathway at the BM stage, but not in peripheral tissue macrophages.

Bone Marrow Transplantation Recovered Macrophage Differentiation and Suppressed Chronic Inflammation and Hypertrophic Gastropathy of the Stomach of Hdc^{-/-} Mice

Peripheral tissue macrophages differentiated from BM cells maintain tissue homeostasis and protect the host from infection.[29] To examine whether BM-derived macrophages are important for gastric homeostasis, normal BM cells of $Hdc^{+/+}$ mice were transplanted to $Hdc^{-/-}$ mice after busulfan administration to generate chimeric mice[30] (Figure 8A). Busulfan removed CD11b+ cells from the BMs and spleen in male mice more efficiently than in female mice, but did not affect the B- or T-cell population (Figure 8B and C). We therefore selected only males for the generation of chimeric mice and related experiments. Flow cytometry showed that transplantation of $Hdc^{+/+}$ BM cells restored the stomach macrophage differentiation in $Hdc^{-/-}$ mice because the number of F4/80+CD11b+ cells regressed to the normal level of the $Hdc^{+/+}$ mouse stomach (Figure 8D). Immunohistochemistry confirmed that the numbers of CD3+ T and F4/80+ cells significantly decreased in the stomachs of $Hdc^{-/-}$ mice after transplantation of $Hdc^{+/+}$ BM cells (Figure 8E and F). Furthermore, the mucosal gland length returned to normal after $Hdc^{+/+}$ BM cell transplantation (G). The phagocytic activity of peritoneal macrophages and stomach macrophages of the $Hdc^{+/+}$ BM cell–transplanted group also recovered (Figure 8H). Consistently, the stomach bacteria could be controlled efficiently after $Hdc^{+/+}$ BM cell transplantation in $Hdc^{-/-}$ mice (Figure 8I), showing that $Hdc^{+/+}$ BM cells rescued the

Figure 1. (*See previous page*). **Naturally occurring hyperplasia and chronic inflammatory region in the histamine-deficient mouse stomach.** (*A*) Naked-eye (*scale bar*: 5 mm) and H&E (*scale bar*: 400 μm) images of the $Hdc^{+/+}$ (n = 5) and $Hdc^{-/-}$ mouse stomach (*left*, n = 13). (*B*) Length of the stomach gland of $Hdc^{+/+}$ and $Hdc^{-/-}$ mice measured at the indicated time points ($Hdc^{+/+}$ n = 5, $Hdc^{-/-}$ n = 13; 25–86 high-power field [HPF] images analyzed per time point). Slides of paraffin sections of the stomachs of 1-year-old $Hdc^{+/+}$ and $Hdc^{-/-}$ mice immunohistochemically stained with (*C*) anti–H+K+-ATPase, (*D*) anti-Ki67, and (*E*) anti-CD3 (*scale bar*: 400 μm; n = 5 mice, 100 H+K+-ATPase+ cells counted in 60 HPF images for Ki67 staining and in 15–20 HPF images for CD3 staining). The H+K+-ATPase+ cell size was determined using the QuPath program (University of Edinburgh). (*F*) Immunofluorescence (IF) staining of GSII (green) and GIF (red) in 1-year-old $Hdc^{+/+}$ and $Hdc^{-/-}$ mouse stomach tissues. Nuclei were stained with 4′,6-diamidino-2-phenylindole (DAPI) (blue). *Scale bar*: 100 μm. Bar graph of the percentage of GIF+ (red), GSII+ (green), and GIF+GSII+ (yellow) cells among total DAPI+ cells in a 10× field (n = 5 mice per group). (*G*) IF staining of GSII (green), CD44v9 (red), and DAPI (blue) in 1-year-old $Hdc^{+/+}$ and $Hdc^{-/-}$ mouse stomach tissues. *Scale bar*: 100 μm. Data are means ± SD. **$P < .01$, ****$P < .0001$. IN, inflammation.
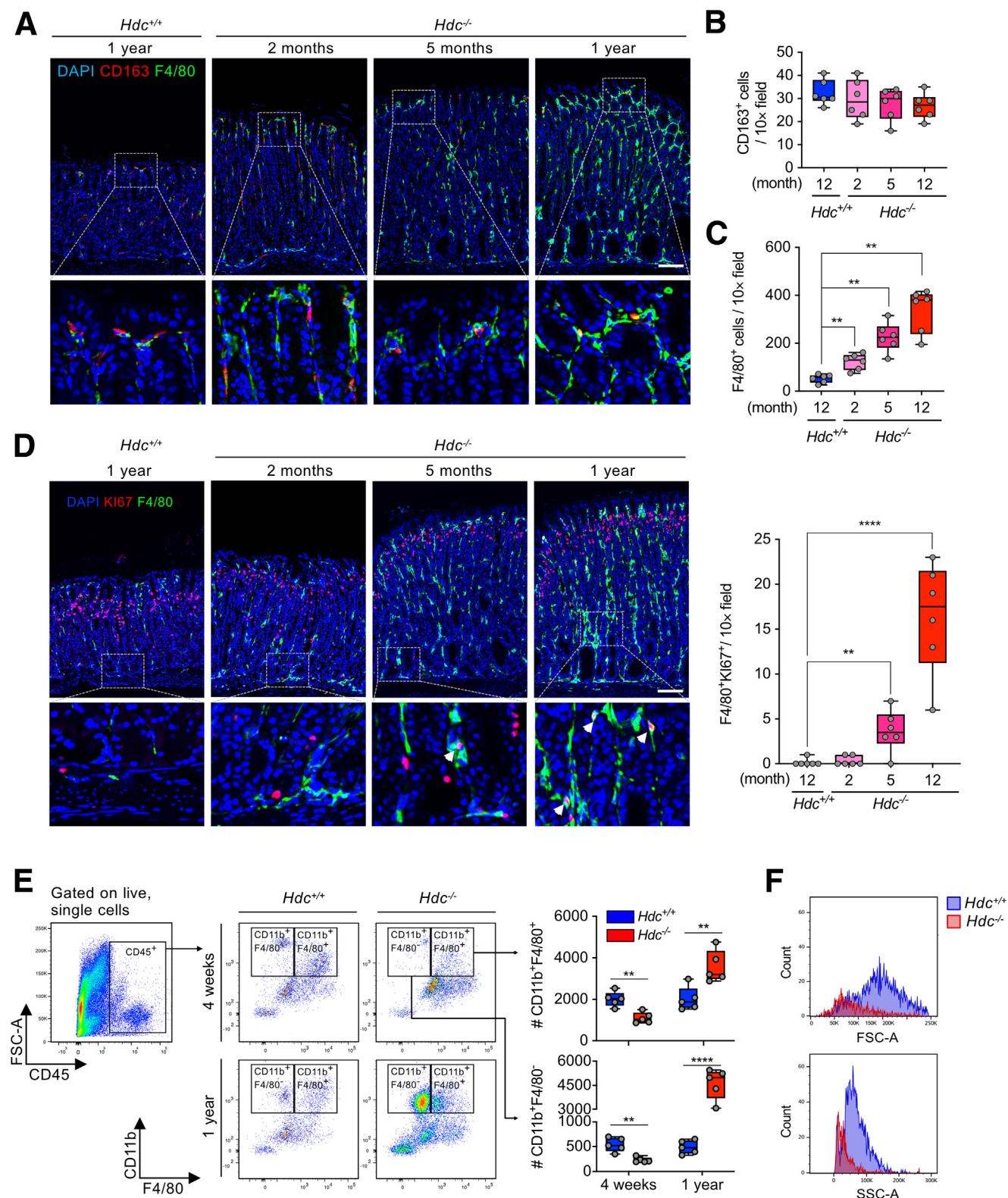
Figure 3. Macrophage phenotype in the histamine-deficient condition. (*A*) Immunofluorescence (IF) staining of CD163 (red), F4/80 (green), and 4′,6-diamidino-2-phenylindole (DAPI) (blue) in the $Hdc^{+/+}$ and $Hdc^{-/-}$ mouse stomach. Quantification of (*B*) CD163$^+$ cells and (*C*) F4/80$^+$ cells in 10× fields. *Scale bar*: 100 μm (n = 6 mice). (*D*) IF staining of Ki67 (red), F4/80 (green), and DAPI (blue) in the $Hdc^{+/+}$ and $Hdc^{-/-}$ stomach. *Left*: Representative IF images. F4/80$^+$Ki67$^+$ cells are highlighted by a *white arrowhead*. *Right*: Bar graph of the number of F4/80$^+$Ki67$^+$ cells in a 10× field. *Scale bar*: 100 μm (n = 6 mice). (*E*) Flow cytometry gating strategy to characterize macrophages in the mouse stomach. $Hdc^{+/+}$ and $Hdc^{-/-}$ mouse stomach cells were first gated on live (DAPI$^-$), single cells, and CD45$^+$ cells. CD45$^+$ cells were distinguished further by CD11b$^+$F4/80$^+$ and CD11b$^+$F4/80$^-$, and the gated populations were calculated (n = 5 mice). (*F*) Comparison of forward scatter-are (FSC-A) and side Scatter-A (SSC-A) levels between the 4-week-old $Hdc^{+/+}$ and $Hdc^{-/-}$ stomach macrophages. Data are shown as means ± SD. **P < .01, ****P < .0001.

differentiation of tissue macrophages of the stomach, which could recover the capacity to suppress bacterial growth and maintain homeostasis of the stomach.

Single-Cell RNA Profiling of Stomach Macrophages of Hdc⁻/⁻ and Hdc⁺/⁺ Mice

To characterize the stomach macrophage phenotype at the molecular level, we conducted single-cell RNA-sequencing (scRNA-seq) of the mucosal stomach cells of 2-month-old *Hdc*⁺/⁺ and *Hdc*⁻/⁻ mice, corresponding to the time that gastric hyperplasia was initiated. After quality control, a total of 25,603 cells (12,303 cells in *Hdc*⁺/⁺ mice and 13,300 cells in *Hdc*⁻/⁻ mice) were analyzed (Figure 9*A*). After batch correction (Figure 9*B*), clustering analysis showed 13 cell clusters (Figure 9*C*), representing pit cells (clusters 1 and 2), isthmus cells (cluster 3), mucous gland cells (cluster 4), chief cells (cluster 5), parietal cells (clusters 6–8), enterochromaffin-like cells (cluster 9), epithelial cells (cluster 10), epithelial stem cells (cluster 11), immune cells (cluster 12), and red blood cells (cluster 13), based on sets of known cell marker genes (Figure 9*D–G*).

Immune cell clusters could be subclustered further into 3 macrophage groups (gastric macrophage 1 [GM1], gastric macrophage 2 [GM2], and gastric macrophage-phagocytic [GMp]), mast cells, T cells, foveolar cells, and fibroblast clusters (Figure 10*A* and *B,* and Supplementary Table 1). Gene set enrichment analysis (GSEA) showed that GM1 was highly associated with M1-type signaling pathways such as tumor necrosis factor-α signaling via nuclear factor-κB and inflammatory response, whereas GM2 was associated with M2-type signaling pathways such as coagulation, hypoxia, adipogenesis, and angiogenesis. It is difficult to characterize the phenotype of GMp cluster because putative M1/M2 polarized signaling pathways could not be determined (Figure 10*C*). These 3 macrophage clusters expressed distinct gene profiles: the GM1 cluster highly expressed *Il1b*, *Mx1*, *Ifnb1*, *Ccl9*, *Cxcl11*, and *Il12b*, and the GM2 cluster expressed *Cd93*, *Pdgfb*, *Ccl24*, *Tnfsf11a*, and *Ccl7*. Interestingly, the GMp cluster was negative for *Adgre1* but highly expressed *CD74*, *H2-Eb1*, *Ppfia4*, *Napsa*, *Cd207*, and *Lsp1*[31] (Figure 10*D*), suggesting that the GMp cluster may have high phagocytic activity. Flow cytometric analysis confirmed that GM1 cells were CD11b⁺F4/80⁺interleukin (IL)1b⁺, which constituted approximately 20% of all CD11b⁺F4/80⁺ cells. GM2 cells were identified to be CD11b⁺F4/80⁺CD93⁺, constituting approximately 60% of all CD11b⁺F4/80⁺ cells. Of note, GMp was negative for F4/80, although GMp cells expressed CD11b and major histocompatibility complex class II (MHCII) (Figure 10*E*). The forward and side scattering results showed that GM1 is a relatively homogenous population among the 3 GM clusters, whereas GM2 is made up of cells with a wide range of size and granularity. The GMp population has a median range of size/granularity between those of the GM1 and GM2 populations (Figure 10*F*). To define the main localizing site of GMp cells in the stomach, 2-month-old stomach tissues were stained immunofluorescently with F4/ 80 and MHCII, showing that F4/80⁻MHCII⁺ GMp cells were enriched at the base and pit region of the stomach fundus

(Figure 10*G*). In addition to F4/80⁺ cells, F4/80⁻MHCII⁺ GMp cells significantly accumulated in the stomachs of 2-month-old and 1-year-old *Hdc*⁻/⁻ mice compared with those of *Hdc*⁺/⁺ mice (Figure 10*H*).
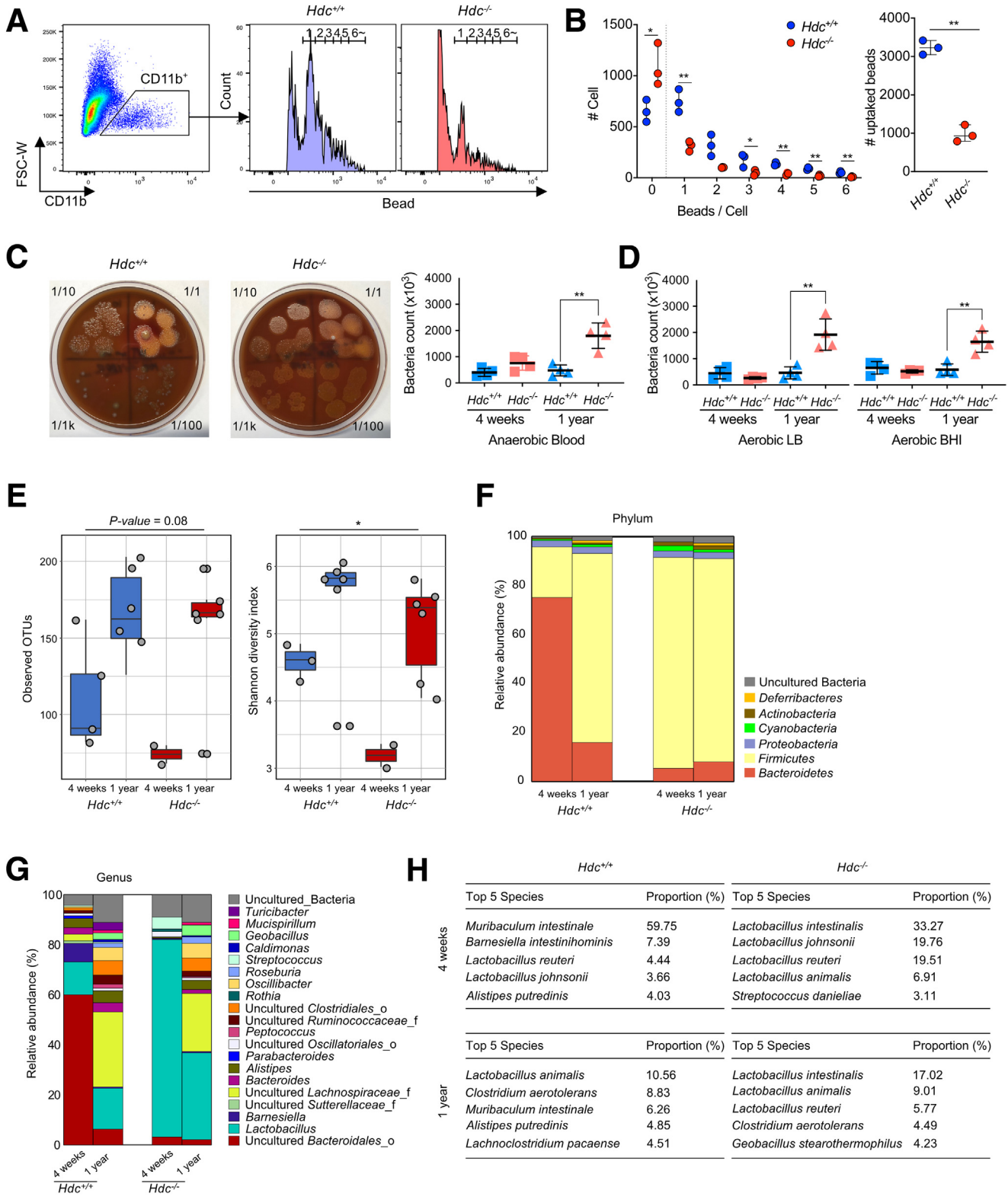
Histamine Deficiency Results in Abnormal Gene Expression and Impaired Phagocytic Activity in All GMs

Consistent with the immunofluorescence staining results (Figure 3*A*), we found an increase in the number of all GMs in the *Hdc*⁻/⁻ mouse stomach (4-fold increase in GM1, 2-fold increase in GM2, and 9-fold increase in GMp) (Figure 11*A*). However, GSEA-based gene ontology analysis showed that gene sets were down-regulated in the GM1 and GM2 clusters of the stomach of *Hdc*⁻/⁻ mice compared with those of *Hdc*⁺/⁺ mice (Figure 11*B*). Consistent with the impaired phagocytic activity of *Hdc*⁻/⁻ stomach macrophages (Figure 4*A*), phagocytosis-related genes tended to be down-regulated in all GM clusters of *Hdc*⁻/⁻ mice compared with those of *Hdc*⁺/⁺ mice (Figure 11*C*). *Helicobacter pylori* is a well-known risk factor for gastric cancer and could cause chronic infection on the mucosal layer of the stomach.[32] To test whether GMs of the stomach of *Hdc*⁻/⁻ mice can properly address *H pylori* infection, murine-adapted *H pylori*–sydney strain 1 (SS1) was labeled with the green fluorescent carboxyfluorescein succinimidyl ester (CFSE) and co-incubated with stomach macrophages; the CFSE signal-positive GMs then were counted. Stomach GMs of *Hdc*⁺/⁺ mice efficiently phagocytosed *H pylori*–SS1 and approximately 60% of GM1, approximately 20% of GM2, and approximately 80% of GMp cells were positive for CFSE. However, all of the stomach GMs of *Hdc*⁻/⁻ mice showed significantly impaired phagocytic activity against *H pylori*–SS1 (Figure 11*D* and *F*). Furthermore, the phagocytic activity of *Hdc*⁻/⁻ GMs also was impaired against *Listeria monocytogenes*[33] or *Shigella flexneri*[34] (Figure 11*E* and *F*).

Phagocytic receptors recognize foreign antigens and induce signaling pathways for phagocytosis.[35] Therefore, we explored whether histamine deficiency alters the expression of phagocytic receptors such as CD64,[36] complement receptor 1/ 2 (CD21/35),[37] CD204 (SR-AI/II),[38] CD14,[39] and V-set immunoglobulin-domain-containing 4 (VSIG4).[40] Flow cytometric analysis showed that the expression of CD21/35 was the most severely impaired among these receptors in all 3 stomach macrophage populations (GM1, GM2, and GMp) in *Hdc*⁻/⁻ mice compared with those of *Hdc*⁺/⁺ mice, and VSIG4 expression also was impaired in the *Hdc*⁻/⁻ GM1 population (Figure 12*A*). To identify whether CD21/35 and VSIG4 are important for phagocytosis in stomach macrophages, GM1, GM2, and GMp cells from *Hdc*⁻/⁻ and *Hdc*⁺/⁺ mice were treated with anti-CD21/35 or anti-VSIG4 for neutralization and then co-incubated with CFSE-labeled *H pylori*–SS1. The complement receptors CD21 and C35 were found to be important for phagocytic activity against *H pylori*–SS1 given that anti-CD21– or anti-CD35–treated GM1 and GMp showed significantly impaired phagocytosis in *Hdc*⁺/⁺ cells. VSIG4 also was found to be required for phagocytosis of *H pylori*–SS1, but only in the GM1 population (Figure 12*B*). However, we could not detect a significant change of phagocytic activity in any *Hdc*⁻/⁻ stomach

macrophage population, even after the treatment of antibodies. This likely is owing to the reduced expression of the receptors in $Hdc^{-/-}$ macrophages, which therefore did not respond to the antibody treatment.

Taken together, these results indicate that histamine is required for the full differentiation of stomach macrophages to maintain stomach homeostasis via phagocytosis of the stomach microbiota.

Discussion

Previous studies have clearly established that histamine deficiency results in hypertrophic gastropathy, including the abnormal proliferation and differentiation of gastric tissue cells.[4,5,17] However, the pathophysiological mechanism underlying the hypertrophic gastropathy of $Hdc^{-/-}$ mice remains unclear. Based on a whole-transcript expression array, we showed that impaired tissue macrophage differentiation and resultant bacterial overgrowth could account for the hypertrophic gastropathy in the HDC-deficiency condition, which was confirmed further by the alleviation of hypertrophic gastropathy with BM transplantation of $Hdc^{+/+}$ mice and GF-$Hdc^{-/-}$ mice. Collectively, these results suggest that histamine signaling might play a critical role in macrophage differentiation and the maintenance of stomach homeostasis through the control of bacterial overgrowth.

With scRNA-seq and flow cytometry, we identified 3 distinct stomach macrophage populations: GM1 (CD11b$^+$F4/80$^+$IL1b$^+$), GM2 (CD11b$^+$F4/80$^+$CD93$^+$), and GMp (CD11b$^+$F4/80$^-$/MHCII$^+$). GSEA showed that GM1 represents classically activated macrophages (M1 type) and GM2 represents alternatively activated macrophages (M2 type) with low phagocytic activity.[41] In addition to these previously known macrophage populations, we newly identified a distinct stomach macrophage population, termed GMp, with high phagocytic activity. Interestingly, compared with $Hdc^{+/+}$ mice, $Hdc^{-/-}$ mice showed increased accumulation of all 3 macrophage populations in the stomach, although the phagocytic activity was decreased, which appeared to be caused by insufficient maturation of macrophages owing to the absence of histamine signaling. The scRNA-seq results supported this speculation because the GM2 cluster was increased by 2-fold in the stomachs of $Hdc^{-/-}$ mice, whereas the number of CD163$^+$ (a known M2-type marker) macrophages did not change significantly, regardless of age or presence of the Hdc gene. Indeed, $Cd163$ gene expression was detected in only a small fraction of GM2 cells (data not shown), suggesting that CD163 may not be a suitable marker for the detection of total stomach M2-type macrophages and that M2 macrophages of various phenotypes may exist in the stomach mucosal tissue to exert different functions such as tissue repair, stem cell regulation, and immune suppression.

The newly identified stomach macrophage population GMp could not be categorized into M1- or M2-type macrophages. However, GMp (CD11b$^+$F4/80$^-$/MHCII$^+$) cells showed high phagocytic capacity comparable with that of GM1 cells, as determined by the phagocytosis assay against 3 bacterial species. GMp did not express the well-known macrophage marker $Adgre1$, but did express $Lsp1$, $Cst3$, Gsn, and highly expressed MHCII-related genes such as $Cd74$, $H2$-Ea-ps, $H2$-$DMb1$, $H2$-Aa, and $H2$-Eb. The gene expression profile of GMp appears to be similar to that of small peritoneal macrophages with an F4/80^{low}MHCII^{high} phenotype. Small peritoneal macrophages are generated from BM-derived myeloid precursors and increase dramatically in response to infectious or inflammatory stimuli,[42] which is a common feature with GMp. Interestingly, histamine deficiency remarkably attenuated the phagocytic activity of GMp, indicating that histamine signaling is pivotal for the functional maturation of GMp compared with that of GM1 or GM2. Therefore, it is conceivable that impaired differentiation of GMp from BM-derived myeloid precursor cells might be accountable for the hypertrophic gastropathy of $Hdc^{-/-}$ mice, although further studies are needed to confirm this possibility.

Various microorganisms can survive in the acidic stomach microenvironment. In particular, H $pylori$ generates urease to neutralize gastric acid and propagates at the mucosal layer of the stomach.[43] Chronic infection with H $pylori$ is a well-known risk factor for chronic gastritis[44] and gastric adenocarcinoma,[45] reflecting the role of infection of microorganisms, including H $pylori$, in the hypertrophic gastropathy of $Hdc^{-/-}$ mice. H $pylori$ infection produces relatively milder inflammatory responses, as determined by minimal increases in tumor necrosis factor-α, IL6, and anti–H $pylori$ IgG levels, and weaker histologic scores in the stomach of $Hdc^{-/-}$ mice compared with that of WT mice,[46] suggesting that histamine is required to initiate immune responses against H $pylori$ infection. Interestingly, GMp macrophages showed the strongest phagocytic activity among GMs against H $pylori$–SS1 (~60% of GM1, ~20% of GM2, and ~80% of GMp cells of $Hdc^{+/+}$ mice underwent phagocytosis), indicating the pivotal role of GMp macrophages for the control of H $pylori$. Of particular note, HDC deficiency reduced the phagocytic activity of GMp to almost one fourth that of $Hdc^{+/+}$ mice, which could explain the bacterial overgrowth and chronic inflammation of the stomach of $Hdc^{-/-}$ mice. Although we showed that CD21/35 and VSIG4 are required for phagocytic activity in GM1, these receptors are not important for phagocytosis in GMp. Therefore, further study is needed to determine the specific substances of GMp that play an important role in phagocytosis.

Figure 4. (*See previous page*). The histamine signal is important for phagocytic activity of stomach macrophages to suppress dysbiosis. (*A*) Phagocytosis assay of $Hdc^{+/+}$ and $Hdc^{-/-}$ stomach macrophages using polystyrene beads. Flow cytometry was performed by gating on live (DAPI$^-$), single cells, CD45$^+$, CD11b$^+$, and beads$^+$. (*B*) The number of beads taken up per CD11b$^+$ macrophage is highlighted, and the total number of beads taken up is calculated. (*C* and *D*) Stomach bacteria numbers. $Hdc^{+/+}$ and $Hdc^{-/-}$ total stomach tissues were homogenized, and serial-diluted tissue samples were plated on blood agar. (*C*) *Left*: Representative blood agar image. *Right*: Expected number of stomach bacteria based on the colony count on blood agar. (*D*) Expected number of stomach bacteria based on the colony count on Luria–Bertani agar (*left*) or brain heart infusion agar (*right*) (n = 4 mice). (*E–H*) 16s ribosomal RNA metagenomic analysis of the stomach tissues of $Hdc^{+/+}$ and $Hdc^{-/-}$ mice. (*E*) Determination of observed operational taxonomic units (OTUs) and Shannon diversity index in the mouse stomach of each group. Relative abundance of the gut microbiota at the (*F*) phylum level and (*G*) genus level. (*H*) Top 5 enriched species are listed for the mouse stomach of each group. Data are shown as means ± SD. *$P < .05$, **$P < .01$. BHI, brain heart infusion; DAPI, 4′,6-diamidino-2-phenylindole; FSC-W, forward scatter-width; LB, luria berani.
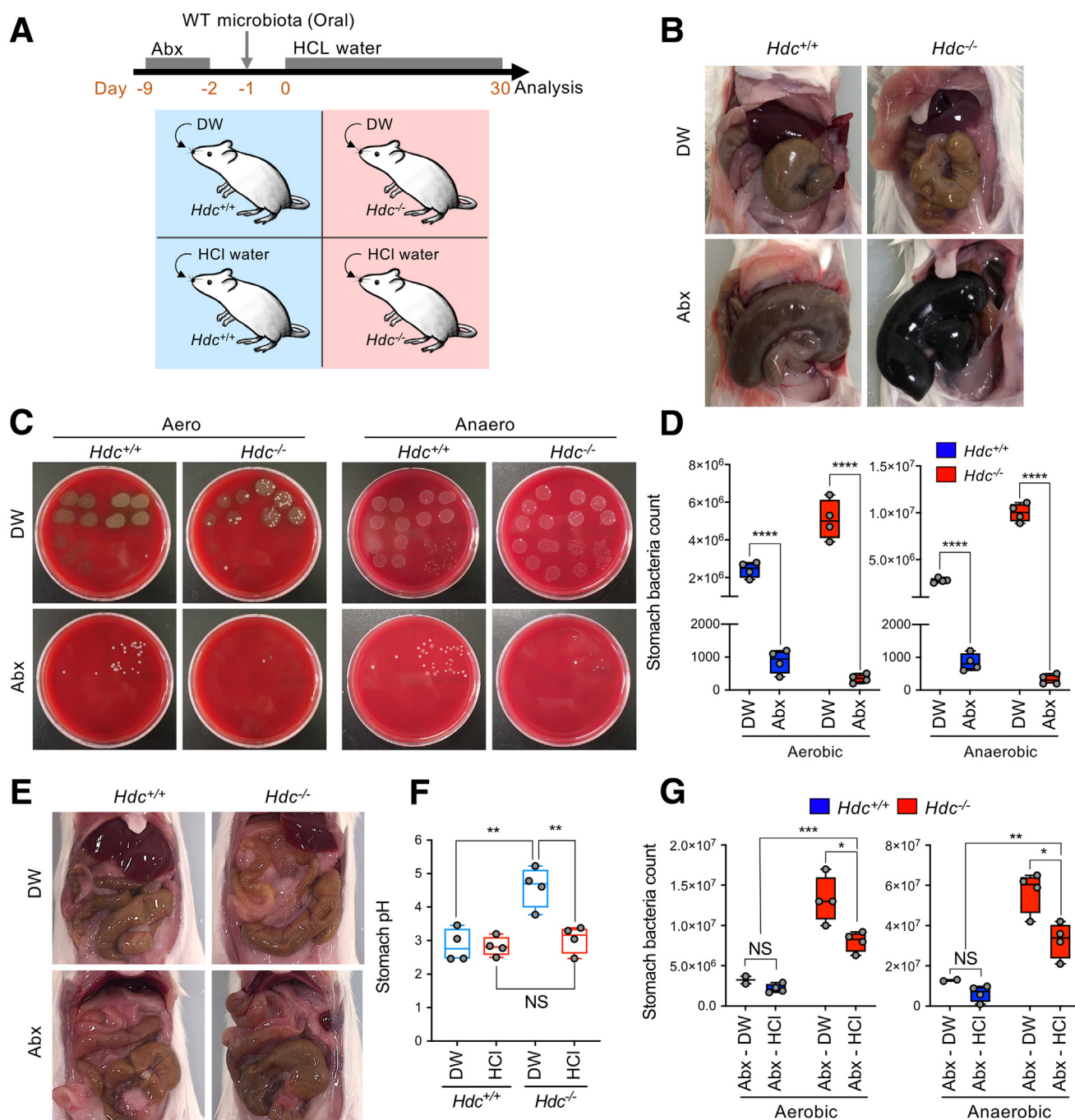
Figure 5. Both acidification and macrophages are important for regulation of stomach bacterial growth. (*A*) Scheme of the experimental design. To define the relation of the pH and bacterial growth in the stomach, 4 different groups of mice were used, as follows: $Hdc^{+/+}$ mice supplied with distilled water (DW) as a control, $Hdc^{+/+}$ mice supplied with HCl-conditioned water, $Hdc^{-/-}$ mice supplied with DW, and $Hdc^{-/-}$ mice supplied with HCl-conditioned water. The microbiota of all groups of mice were removed by administration of an antibiotics cocktail (ABX). (*B*) ABX efficiency test. Each group of mice was killed after treatment of ABX or DW for 7 days and imaged after opening the abdominal cavity. (*C*) The total stomach tissue of each group was homogenized and plated on blood agar as described in Figure 4*G*. Representative blood agar image in each group. (*D*) Expected stomach bacteria number in each group by counting the colonies on blood agar. *Left*: Cultured in aerobic condition. *Right*: Cultured in anaerobic condition (n = 4 mice). (*E–G*) ABX-treated mice were supplied with control DW or HCl-conditioned water for 30 days. (*E*) Four groups of mice were killed and imaged after opening the abdominal cavity. (*F*) pH of the stomach mucosal tissue. Box-and-whisker plot. (*G*) Expected stomach bacteria number in each group was determined by counting the colonies on blood agar. *Left*: Cultured in aerobic condition. *Right*: Cultured in anaerobic condition (n = 4 mice). (*D* and *G*) Results are presented as means ± SD. *P < .05, **P < .01, ***P < .001, ****P < .0001. NS, not significant by 2-way analysis of variance.
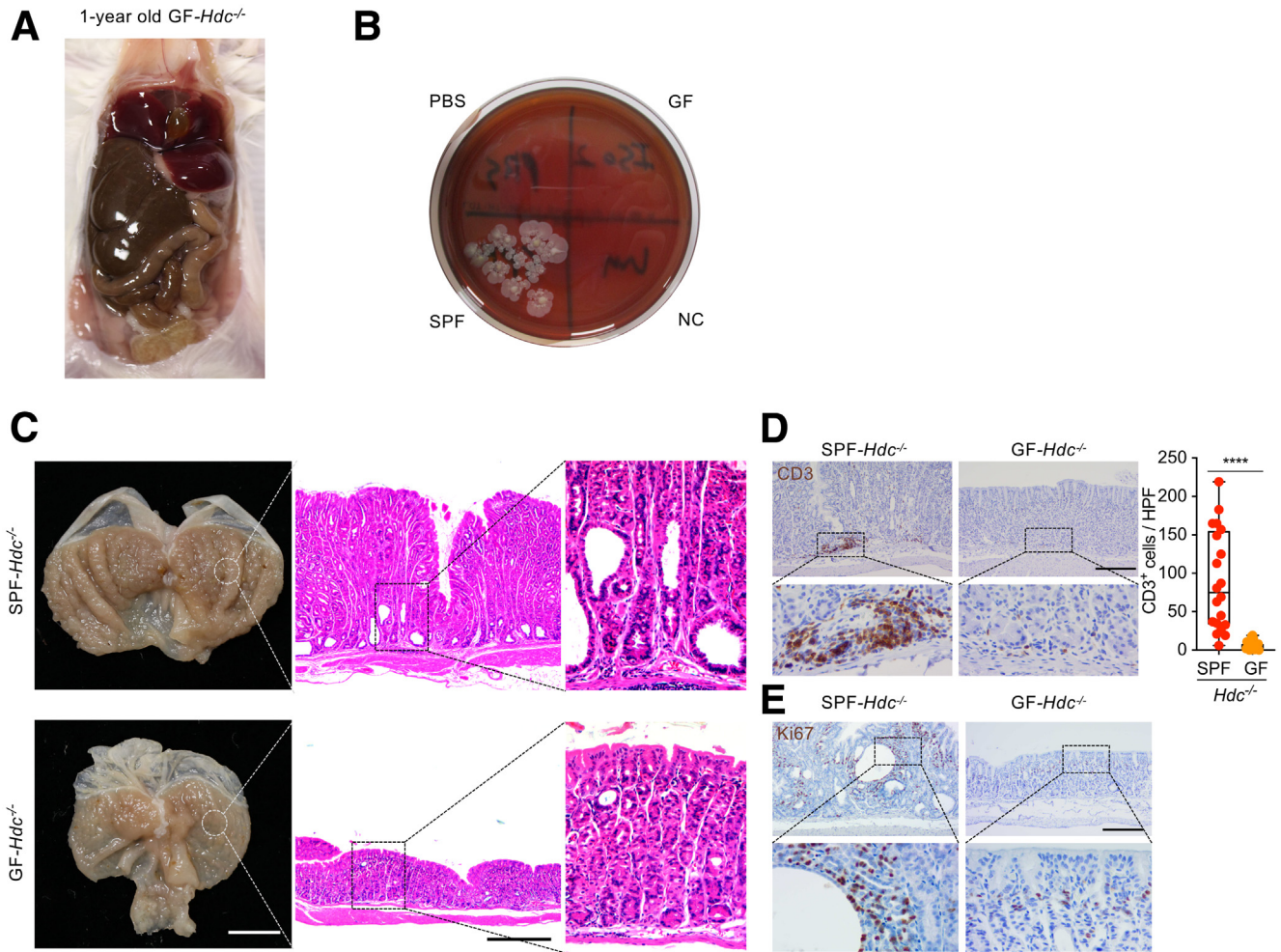
Figure 6. Chronic inflammation and hypertrophic gastropathy did not occur in GF *Hdc*^{-/-} mice. (*A*) One-year-old GF *Hdc*^{-/-} mice were killed and imaged after opening the abdominal cavity. (*B*) Feces from SPF *Hdc*^{-/-} and GF *Hdc*^{-/-} were suspended in sterile PBS. Each group of samples was plated on blood agar and cultured for 2 days in an anaerobic condition. (*C*) Gross and H&E-stained images of the 1-year-old SPF *Hdc*^{-/-} and GF-*Hdc*^{-/-} mouse stomach. *Scale bars*: 5 mm and 400 μm, respectively. (*D* and *E*) Immunohistochemical images and quantification of (*D*) CD3^{+} cells and (*E*) Ki67^{+} cells in 1-year-old SPF *Hdc*^{-/-} and GF *Hdc*^{-/-} mouse stomachs. Data are shown as means $\pm$ SD. *Scale bars*: 0.2 mm. ****$P <$ .0001. GF, feces from GF *Hdc*^{-/-} mice; NC, negative control; PBS, sterile PBS only; SPF, feces from SPF *Hdc*^{-/-} mice.

Histamine regulates various types of macrophages via different receptors. For example, histamine promotes the quiescence and self-renewal of hematopoietic stem cells via the H$_2$-receptor signaling pathway,[11] and H$_4$-receptor signaling enhances the phagocytic activity of BM-derived macrophages.[23] In line with these reports, we showed that the impaired differentiation and phagocytic activity of *Hdc*^{-/-} BM cells were recovered by histamine treatment, underlining the importance of histamine signaling in the functional maturation of stomach tissue macrophages from BM cells. Consistently, treatment of GMCSF and CSF-1 to BM cells of *Hdc*^{+/+} mice stimulated the production of histamine, whereas the BM cells of *Hdc*^{-/-} mice were unresponsive to this treatment, suggesting that the source of histamine for the differentiation of tissue macrophages in the stomach may be BM cells. Indeed, transplantation of BM cells from *Hdc*^{+/+} mice to *Hdc*^{-/-} mice recovered normal macrophage differentiation and phagocytic activity, which may have contributed to the control of bacterial overgrowth and the maintenance of gastric homeostasis.

In conclusion, we showed that histamine signaling is important for tissue macrophage differentiation and maintenance of gastric homeostasis through the suppression of bacterial overgrowth in the stomach. Moreover, this study provides new insight into the mechanism of pathogenesis of hypertrophic gastropathy mediated by bacterial overgrowth from impaired macrophages, which can contribute toward understanding the development of various inflammatory gastric diseases and aiding in the discovery of new therapeutic strategies.

Materials and Methods
Lead Contact

Further information and requests for resources and reagents should be directed to and will be fulfilled by the lead contact, Ki Taek Nam. KITAEK@yuhs.ac
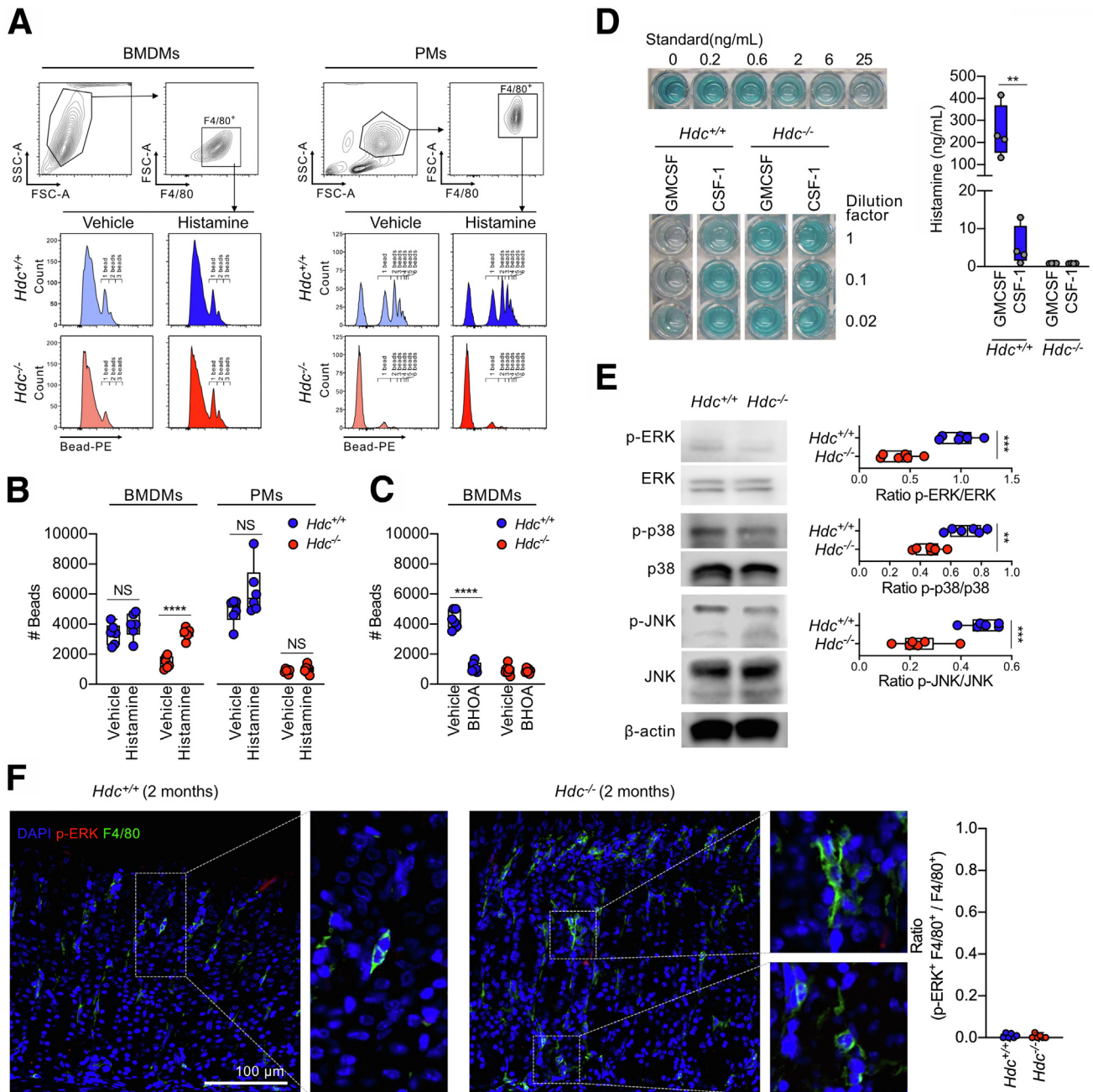
Figure 7. MAPK signaling is impaired in *Hdc*⁻/⁻ mouse BM cells, but not in stomach macrophages. (*A* and *B*) BMDMs from 4-week-old *Hdc*⁺/⁺ and *Hdc*⁻/⁻ mice were incubated in GMCSF–supplemented media and 10^{-6} mol/L histamine the same day. On day 7, the F4/80⁺ cells were gated and a phagocytosis assay was performed. (*A*) Peritoneal cells from 4-week-old *Hdc*⁺/⁺ and *Hdc*⁻/⁻ mice were treated with 10^{-6} mol/L histamine for 2 days in vitro and a phagocytosis assay was performed. (*B*) Quantification of the total number of phagocytosed beads in each group (n = 6 mice). (*C*) BMDMs from 4-week-old *Hdc*⁺/⁺ and *Hdc*⁻/⁻ mice were incubated in GMCSF–supplemented media with or without 4-bromo-3-hydroxybenzoic acid (BHOA) the same day. On day 7, the F4/80⁺ cells were gated and a phagocytosis assay was performed. (*D*) Four-week-old *Hdc*⁺/⁺ and *Hdc*⁻/⁻ GMCSF–treated BMDMs and CSF-1–treated BMDMs were cultured for 7 days. The histamine level in each group in the culture supernatant was determined using an enzyme-linked immunosorbent assay (n = 4 mice). (*E*) BM cells from *Hdc*⁺/⁺ and *Hdc*⁻/⁻ mice were lysed and Western blot was performed with antibodies specific for phospho-ERK (p-ERK), ERK, phospho-p38 (p-p38), p38, phospho-JNK (p-JNK), JNK, and β-actin. Results are presented as means ± SD (n = 6 mice). (*F*) Immu-nofluorescence staining of p-ERK (red), F4/80 (green), and 4′,6-diamidino-2-phenylindole (DAPI) (blue) in the *Hdc*⁺/⁺ and *Hdc*⁻/⁻ mouse stomach (n = 6 mice). *Scale bar*: 100 μm. **P < .01, ***P < .001, ****P < .0001. FSC-A, forward scatter-area; PM, peritoneal macrophage; SSC-A, side scatter-area.

Mice

Animal experiments were approved by the Institutional Animal Care and Use Committee of Yonsei University (2015-0116) and were compliant with the Guide for the Care and Use of Laboratory Animals. Wild-type FVB/NJ friend virus b NIH Jackson (FVB/NJ) mice were purchased from The Jackson Laboratory (Bar Harbor, ME) and $Hdc^{-/-}$ mice were a kind gift from Dr Timothy C. Wang (Columbia University, New York, NY). The mice were maintained in a SPF barrier and GF facility under a 12-hour light cycle, and provided PicoLab Rodent Diet 20 (LabDiet, St. Louis, MO) for the SPF condition and Teklad Global 18% Protein Rodent Diet (Envigo, Indianapolis, IN) for the GF condition. GF-$Hdc^{-/-}$ mice were generated according to previously reported methods.[47,48] $Hdc^{-/-}$ mice were maintained by crossing $Hdc^{+/-}$ mice. Four weeks after birth, the offspring were separated from the mother's cage and genotyped with primers $Hdc^{+/+}$_Sense (GAGCACTGTCAGCGAATCCAC), $Hdc^{+/+}$_Antisense (GGCCGTGAGATAAGCGTGACC), and $Hdc^{-/-}$_Antisense (TGGGATTAGATAAATGCCTGCTCT). The $Hdc^{+/+}$ and $Hdc^{-/-}$ mice used in the spontaneous stomach hyperplasia study were 2–12 months old, and 4-week-old mice were used in the other experiments (scRNA-seq analysis, macrophage characterization, and generation of chimeric mice). All individual experiments involved sex matching and approximately the same numbers of male and female mice were used in the overall experiment; however, only male mice were used in the scRNA-seq analysis and for the experiments with chimeric mice.

H&E Staining and Stomach Gland Length

The mouse stomach was fixed with ice-cold 4% paraformaldehyde and then embedded in paraffin. The tissues were sectioned at a thickness of 5 μm, deparaffinized with xylene 3 times for 20 minutes each, 100% ethanol 3 times for 10 minutes each, 90% ethanol twice for 10 minutes each, and 75% ethanol for 10 minutes, and then stained with H&E-stained tissue slides were dehydrated using by ethanol xylene, and mounted with Shandon Synthetic Mount (Thermo). The length of the stomach mucosal gland was determined by taking the average of approximately 25 glands per mouse from digital images using the ToupView program (http://www.touptek.com).

Immunohistochemical and Immunofluorescence Staining

For immunohistochemistry, the tissues were fixed with ice-cold 4% paraformaldehyde in phosphate-buffered saline (PBS) and mounted in paraffin blocks. Samples were sectioned at 3 μm, deparaffinized, and rehydrated in PBS. Antigens then were retrieved for 15 minutes under high pressure in Target Retrieval Solution (Dako). Subsequently, the specimens were chilled on ice for 1 hour, washed with PBS 3 times for 5 minutes each, and blocked with 3% H_2O_2 in PBS for 30 minutes to quench the endogenous peroxidase. The slides were washed again with PBS, blocked for 2 hours at room temperature with Serum-Free Protein Block (Dako), probed at 4°C overnight with the primary antibodies (1/1000 dilution), stained for 30 minutes with anti-mouse (Dako) or horseradish peroxidase–conjugated anti-rabbit IgG (Dako) secondary antibody, and developed with Liquid DAB+ Substrate Chromogen System (Dako). Finally, the specimens were counterstained with Mayer's hematoxylin (Dako) and mounted with Shandon Synthetic Mount (Thermo).

For immunofluorescence, tissue sample preparation and blocking were performed in the same manner as described earlier for immunohistochemistry, probed at 4°C overnight with the primary antibodies (1/1000 dilution), labeled for 2 hours with cyanine-3 (Cy3)-conjugated goat anti-rabbit-IgG (Invitrogen) or A488 donkey anti-rat lgG (Invitrogen), and stained with 4′,6-diamidino-2-phenylindole (Sigma) for 15 minutes. Finally, the slides were mounted with ProLong Gold antifade reagent (Invitrogen), imaged on an LSM 700 confocal microscope (Zeiss), and analyzed using Zeiss Zen Blue Edition.

The following primary antibodies were used: anti-Ki67 (ab16667; Abcam), anti–H^+K^+ ATPase (D031-3; MBL), anti-CD3 (ab5690; Abcam), anti–GSII-a488 (L21415; Thermo), anti-GIF (Dr David Alpers), anti-CD44v9 (CAC-LKG-M002; Cosmo Bio), anti-CD163 (NB110-59935SS; Novus), anti-F4/80 (ab6640; Abcam and D2S9R; Cell Signaling Technology), and anti-MHCII (NBP2-21798; Novus).

## Whole-Transcript Expression Array

One-year-old mouse stomach tissues were homogenized by T-10 basic ULTRA-TURRAX (IKA, Staufen, Germany) in TRIzol reagent, and RNA was isolated according to the manufacturer's instructions (Invitrogen). For quality control, the RNA purity and integrity were evaluated according to the optical density ratio at 260/280 nm using an ND-1000 spectrophotometer (NanoDrop, Wilmington, DE) and analyzed with an Agilent 2100 Bioanalyzer (Agilent Technologies, Palo Alto, CA). The Affymetrix whole-transcript expression array process was executed according to the manufacturer's protocol (GeneChip Whole Transcript PLUS reagent Kit; Affymetrix). Complementary DNA (cDNA) was synthesized using the GeneChip Whole Transcript Amplification kit as described by the manufacturer. The sense cDNA then was fragmented and biotin-labeled with terminal deoxynucleotidyl transferase using the GeneChip Whole Transcript Terminal labeling kit. Approximately 5.5 μg labeled DNA target was hybridized to the Affymetrix GeneChip Human or Mouse 2.0 ST Array at 45°C for 16 hours. Hybridized arrays were washed and stained on a GeneChip Fluidics Station 450, and then scanned on a GCS3000 Scanner (Affymetrix). Signal values were computed using Affymetrix GeneChip Command Console Software (AGCC).

Raw data were extracted automatically in the Affymetrix data extraction protocol using Affymetrix AGCC. After importing CEL files, the data were summarized and normalized with the robust multi-average method implemented in the oligo package[49] in Affymetrix Power Tools for differentially expressed gene (DEG) analysis (Supplementary Table 2).

Statistical significance of the expression data was determined using the local-pooled-error (LPE) test and fold change in which the null hypothesis was that there is no difference between groups. The false discovery rate was

controlled by adjusting the P value ($P < .05$) using the Benjamin–Hochberg algorithm. For the obtained DEG set, hierarchical cluster analysis was performed using complete linkage and the Euclidean distance as a measure of similarity.

Gene enrichment and functional annotation analysis for the significant gene list were performed using Gene Ontology (http://geneontology.org) and Kyoto Encyclopedia of Genes and Genomes (http://kegg.jp) tools with
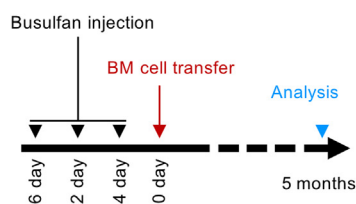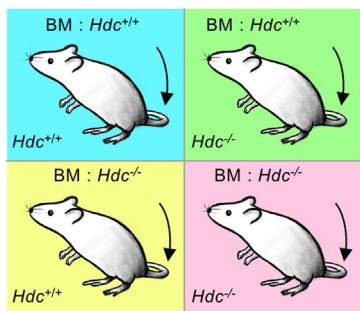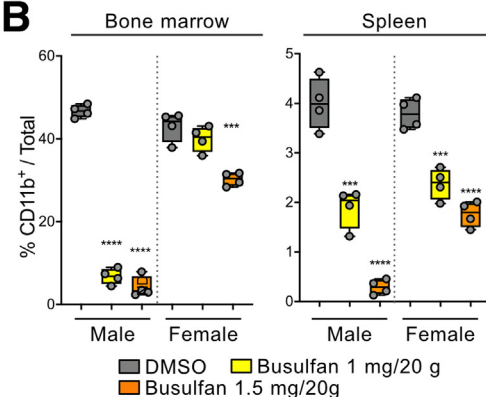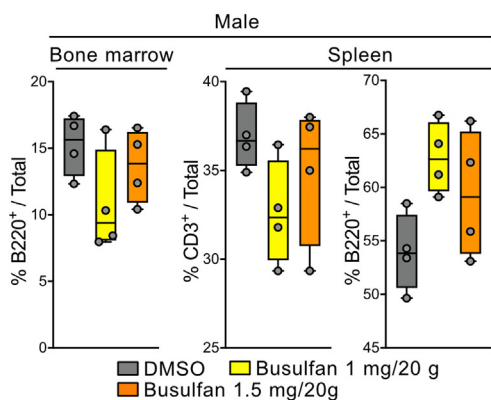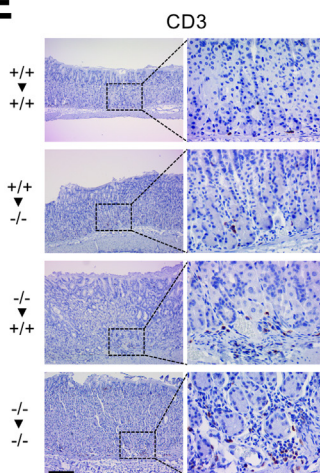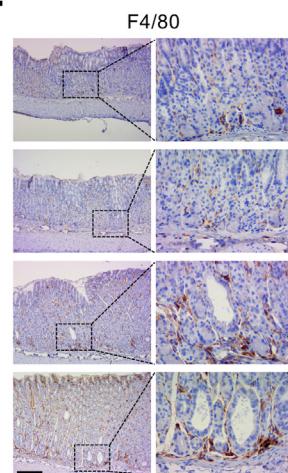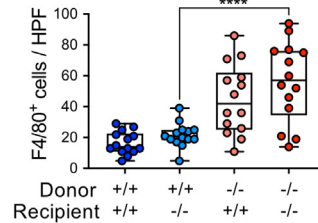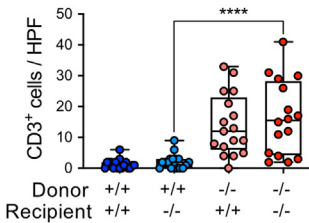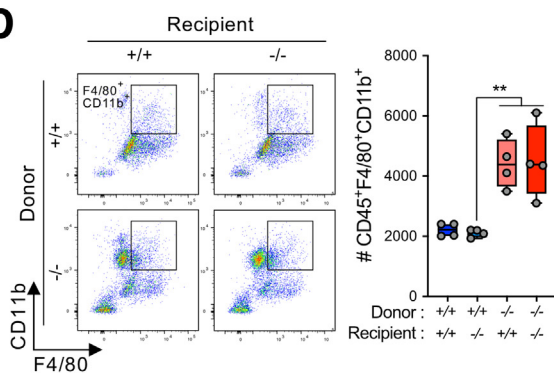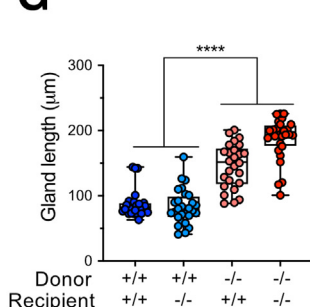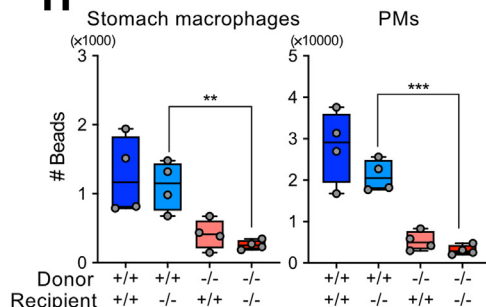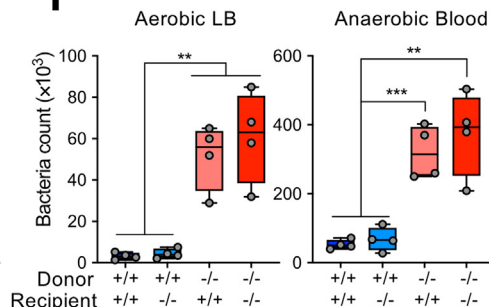
representative oligonucleotide microarray analysis[50] and HALLMARK.[51] An immune cell population was estimated using CIBERSORT[21] and immuCC.[52] All statistical tests and visualization of DEGs were conducted using R statistical language v. 3.5.3 (www.r-project.org). Raw sequencing data have been submitted to GEO repository (GSE213293).

Stomach Single-Cell Isolation and Preparation

Mice were killed using CO_2 gas, and total mouse stomach tissues were obtained by cutting the distal region of the esophagus and the proximal region of the duodenum. To remove the contents of the stomach, the greater curvature was cut and washed with PBS twice. The forestomach was removed and the tissues were cut into approximately 1-mm³ pieces. The stomach tissue was incubated in 50 mL solution A (0.5 mmol/L NaH_2PO_4, 1 mmol/L Na_2HPO_4, 20 mmol/L $NaHCO_3$, 70 mmol/L NaCl, 5 mmol/L KCl, 50 mmol/L HEPES, 11 mmol/L D-[+]-glucose, 2 mmol/L EDTA, 2% bovine serum albumin, and 0.2 mg pronase E) in a 37°C shaking incubator for 30 minutes. The stomach tissue then was moved to 50 mL solution B (0.5 mmol/L NaH_2PO_4, 1 mmol/L Na_2HPO_4, 20 mmol/L $NaHCO_3$, 70 mmol/L NaCl, 5 mmol/L KCl, 50 mmol/L HEPES, 11 mmol/L D-[+]-glucose, 1 mmol/L $CaCl_2$, 1.5 mmol/L $MgCl_2$, 2% bovine serum albumin, and 0.2 mg pronase E) and incubated for 2 hours in a 37°C shaking incubator. To obtain the single suspended total stomach cell, solution A and solution B were filtered using a 40-μm cell strainer (352340; CORNING) and centrifuged at 1000 rpm for 10 minutes. The cell pellet was resuspended in RPMI-1640 medium with 10% fetal bovine serum (FBS) for in vitro experiments.

qPCR

The mouse stomach tissue was homogenized by T-10 basic ULTRA-TURRAX (IKA) in TRIzol reagent, and RNA was isolated according to the manufacturer's instructions (Invitrogen). Reverse-transcription qPCR was performed in triplicate in 96-well plates using Power SYBR Green PCR Master Mix (Thermo) on a StepOnePlus Real-Time PCR System (Applied Biosystems, Darmstadt, Germany) (*Il1b*-F: 5'-ACGGACCCCAAAA-GATCAAGGGCT-3', *Il1b*-R: 5'-CCTGGAAGGTCCACGGGAAA-GAC-3', *Tnfa*-F: 5'-ACCCTCACACTCAGATCATC-3', *Tnfa*-R: 5'-GAGTAGACAAGGTACAACCC-3', *Cd80*-F: 5'-CCATGTC-CAAGGCTCATTCT-3', *Cd80*-R: 5'-GGCAAGGCAGCAATACCTTA-3', *Cd86*-F: 5'-TCAGTGATCGCCAACTTCAG-3', *Cd86*-R: 5'-TTAGGTTTCGGGTGACCTTG-3', *Nos2*-F: 5'-GCCACCAA-CAATGGCAACA-3', *Nos2*-R: 5'-CGTACCGGATGAGCTGTGAATT-3', *Il4*-F: 5'-CACAGGAGAAGGGACGCCATGC-3', *Il4*-R: 5'-ATGC-GAAGCACCTTGGAAGCCC-3', *Il13*-F: 5'-GCTCTGGGCTTCAT GGCGCT-3', *Il13*-R: 5'-AGGGCTACACAGAACCCGCCA-3', *Il10*-F: 5'-GGTTGCCCAGCCTTATCGGA-3', *Il10*-R: 5'-ACCTGCTCCACTG CCTTGCT-3', *Arg1*-F: 5'-AGGACAGCCTGGAGGAGGGG-3', *Arg1*-R: 5'-TGGACCTCTGCCACCACACCAG-3', and *Ym1*-F: 5'-GGGCATACCTTTATCCTGAG-3', *Ym1*-R: 5'-CCACTGAAGT-CATCCATGTC-3'). Relative messenger RNA levels were calculated according to the $\Delta\Delta CT$ relative quantification method and were normalized to the level of the housekeeping gene *Gapdh*.

Flow Cytometry

The mouse stomach cells were blocked with 2 $\mu L/10^6$ cells of Fc Block (BD) in 100 μL fluorescence-activated cell sorter (FACS) buffer (0.5% FBS, 1 mmol/L EDTA, 0.05% NaN_3 in PBS) for 10 minutes at 4°C, followed by washing with FACS buffer to remove Fc Block residue. Cell surface staining was performed in FACS buffer containing antibody cocktails (PerCP [Peridinin chlorophyll]/Cy [Cyanine] 5.5-CD45, APC [Allophycocyanin]/Cy7-CD11b, and APC-F4/80; PerCP/Cy5.5-CD45, APC/Cy7-CD11b, APC-F4/80, Pacific Blue–MHCII, and PE/Cy7-CD93; PerCP/Cy5.5-F4/80, APC/Cy7-CD11b, Pacific Blue–MHCII, PE/Cy7-CD93, APC-CD64, APC-CD21/35, APC-CD204, APC-CD14, and APC-VSIG4) on ice for 1 hour. After washing with FACS buffer 3 times, the cells were subjected to flow cytometry with a BD LSR Fortessa cytometer and data were analyzed with FlowJo software.

For intracellular staining, the Fc-blocked cell surface was stained with antibody cocktails on ice for 1 hour. After washing with FACS buffer, the cells were fixed using Cyto-fix/Cytoperm solution (BD) for 20 minutes on ice, followed by washing with Perm/Wash solution (BD). Intracellular staining was performed using PE-Il1β (BioLegend) for 1 hour on ice. The cells were washed again with Perm/Wash solution twice and analyzed by flow cytometry using a BD LSR Fortessa cytometer.

16S Ribosomal RNA Metagenomic Analysis

Bacterial DNA was extracted using the PowerMax Soil DNA Isolation Kit (12988-10; MO BIO). The quality of the extracted genomic DNA was validated according to the absorbance ratio at 260 nm and 280 nm (A260/280) using

Figure 8. (*See previous page*). **Generation of chimeric mice and recovery of macrophage activity.** (*A*) Scheme of the experimental design. (*B* and *C*) Busulfan-mediated depletion of macrophages in the BM and spleen. Four-week-old FVB male and female mice were injected with dimethyl sulfoxide (DMSO; vehicle control) or various doses of busulfan via the intraperitoneal route, 3 times every 2 days. Flow cytometry of total BM cells and splenocytes was performed, first gating on live (DAPI⁻), single, and CD45⁺ cells, and then further gating by CD11b, B220, or CD3. (*D*) Flow cytometry of stomach macrophages in chimeric mice. Total stomach cells were first gated on live (DAPI⁻), single, and CD45⁺ cells, and further distinguished by the relative expression of CD11b and F4/80 in each group (n = 4 mice). Stomach tissues were stained immunohistochemically with (*E*) anti-CD3 and (*F*) anti-F4/80. CD3⁺ and F4/80⁺ cells were counted in high-power fields (HPFs). *Scale bar*: 200 μm (n = 4 mice and 14–17 HPF images). (*G*) Length of the stomach mucosal gland presented as a box-and-whiskers plot (n = 4 mice and 32 HPF images analyzed). (*H*) Stomach macrophages (*left*) and peritoneal macrophage (PMs) (*right*) incubated with polystyrene beads and subjected to a phagocytosis assay (n = 4 mice). (*I*) Stomach bacterial numbers. *Left*: Number of colonies on Luria–Bertani plates in an aerobic condition. *Right*: Number of colonies on blood agar plates in an anaerobic condition (n = 4 mice). (*B–D*, *G*, and *H*) Results are presented as means ± SD. **P < .01, ***P < .001, ****P < .0001. DAPI, 4′,6-diamidino-2-phenylindole; LB, luria berani.
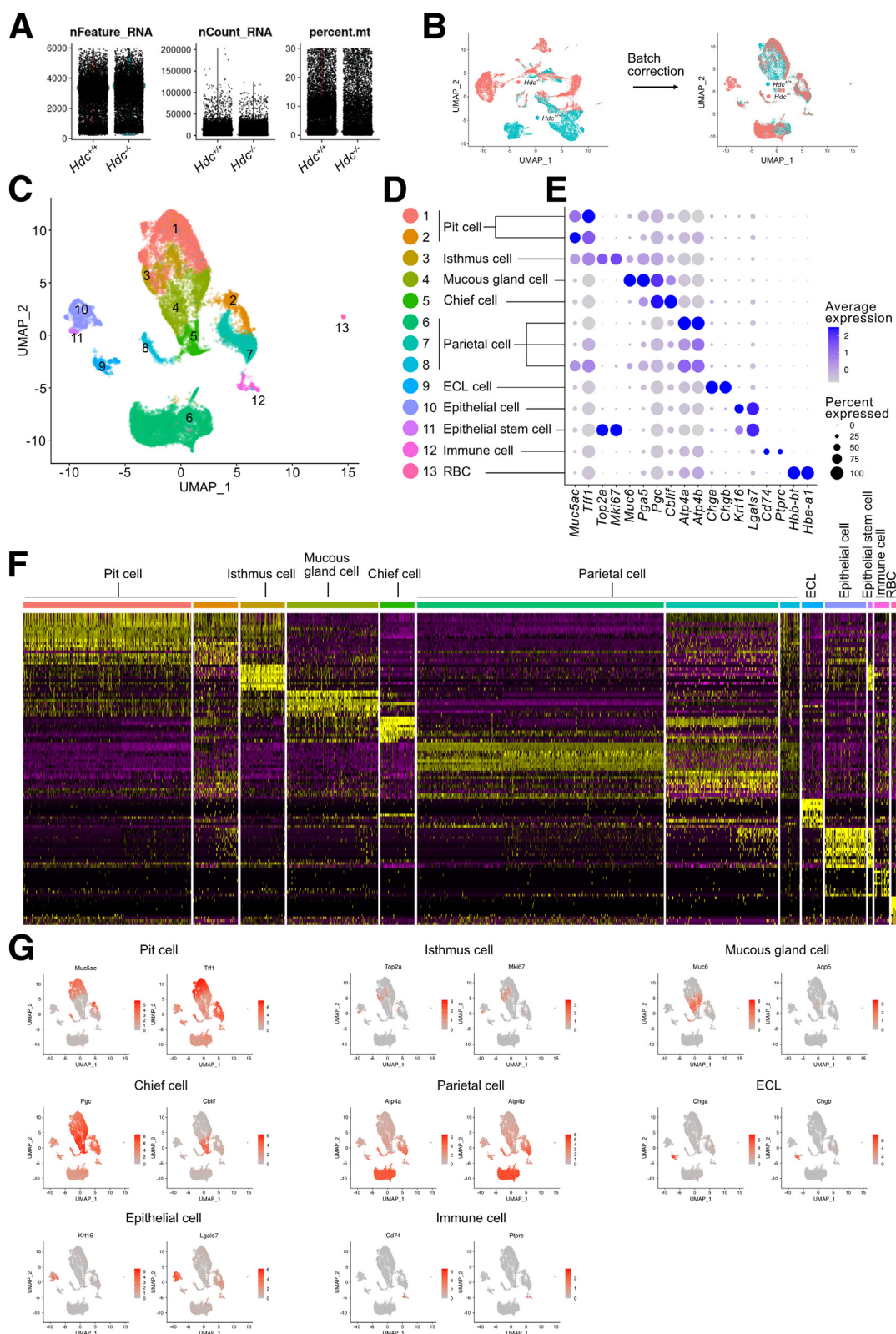
Figure 9. scRNA-seq analysis of the mouse stomach. (*A*) Violin plots showing the number of features, the number of read counts, and the percentage of mitochondria genes in individual cells. (*B*) Batch correction of uniform manifold approximation and projection (UMAP) between *Hdc*$^{+/+}$ and *Hdc*$^{-/-}$ stomach cells. (*C*) UMAP from 2-month-old mouse *Hdc*$^{+/+}$ and *Hdc*$^{-/-}$ stomach cells. (*D*) Identification of assigned cell types. Clusters 1 and 2, pit cells 1 and 2 respectively; cluster 3, isthmus cells; cluster 4, mucous gland cells; cluster 5, chief cells; clusters 6–8, parietal cells 1–3 respectively; cluster 9, enterochromaffin-like (ECL) cells; cluster 10, epithelial cells; cluster 11, epithelial stem cells; cluster 12, immune cells; and cluster 13, red blood cells (RBCs). (*E*) Average expression levels (color scheme) and percentage of cells (spot size) expressing the top genes across the 13 clusters. (*F*) Heat map of differentially expressed genes for each cluster with an area under the receiver operating curve cut-off value ≥0.85. (*G*) UMAP plots showing the expression patterns of cell-type–specific marker genes.

an Epoch spectrophotometer (Biotek, Winooski, VT). The concentration of genomic DNA was determined on a Pico-Green system (P11496; Invitrogen), and the quality was validated further by gel electrophoresis.

16S ribosomal DNA amplicons were amplified with a bacterial primer pair[53] containing a forward overhang adapter sequence (341F: 5'-CCTACGGGNGGCWGCAG-3', 805R: 5'-GACTACHVGGGTATCTAATCC-3'). The first PCR mixture included Herculase 5× Reaction Buffer, deoxy-nucleoside triphosphate mixture (25 mmol/L each), 1 U Herculase II polymerase (600677; Agilent), 5 mmol/L overhang primers, and 10 ng template DNA, and amplifica-tion was performed with the following program: 95°C for 3 minutes (initial denaturation); 25 cycles of 95°C for 30 seconds (denaturation), 55°C for 30 seconds (annealing), and 72°C for 30 seconds (extension); and final extension at 72°C for 5 minutes. The amplicon obtained from this first PCR was purified using Agencourt AMPure XP Reagents beads (A63881; Beckman). The second PCR mixture included Herculase 5× Reaction Buffer, deoxynucleoside triphosphate mixture (25 mmol/L each), 1 U Herculase II polymerase, Nextera XT Index Primer (FC-131-1001; Illu-mina, San Diego, CA), and 5 mL amplicon obtained from the first PCR; amplification was performed according to the same conditions described earlier except that 10 cycles were used from denaturation to extension. The amplicon obtained from this second PCR also was purified using Agencourt AMPure XP Reagents beads. The length and concentration of PCR amplicons were determined using Bioanalyzer 2100 (Agilent Technologies, Palo Alto, CA), and sequencing was performed using a MiSeq 250 paired-end system (Illumina) according to the manufacturer's manual.

FASTQ files were generated from MiSeq raw data using Real Time Analysis and bcl2fastq (v2.20.0.422). Paired-end data in each sample were assembled to a single sequence using FLASH (v1.2.11).[54] Obtained sequences were analyzed using the CD-HIT (cluster database at high identity with tolerance)-EST–based CD-HIT-OTU[55] program for removing error sequences such as low-grade, ambiguous, and chimera sequences. After removing the error sequences, the total species level of operational taxonomic units was generated by clustering sequences with a similarity threshold of 97%. Representative sequences in each operational taxonomic unit were analyzed by BLASTN (v.2.4.0)[56] and taxonomic assignment was performed according to the National Center for Biotechnology Information 16S Microbial reference database. However, we did not identify taxa with a query coverage lower than 85% according to the reference data-base and sequence identity lower than 85% for matched domains. Raw sequence data have been deposited in the NCBI Sequence Read Archive database (BioProject ID: PRJNA880436).

Generation of BMDMs

The femurs were obtained from 4-week-old $Hdc^{+/+}$ and $Hdc^{-/-}$ mice. The epiphyses of the bones were removed with sterile scissors and the BM was flushed out with a 26G needle syringe filled with PBS. BM cells were centrifuged at 494 × g for 5 minutes and resuspended in BMDM medium (RPMI 1640, 10% FBS, 100 μg/mL streptomycin, and 100 U/mL penicillin) with 100 ng/mL GMCSF. The cells then were seeded on 12-well plates and cultured in a 37°C, 5% CO$_2$ incubator for 7 days. Three days after cell seeding, the cell culture plate was replaced with fresh BMDM medium.

Phagocytosis Assay, Complement Opsonization, and CFSE Labeling of Bacteria

Stomach cells were suspended in RPMI-1640 (5% FBS) medium at 2×10^5 cells/mL. Each group of cells was seeded on 12-well plates and incubated for 6 hours in a 37°C, 5% CO$_2$ incubator. Then 1.0-μm FluoSpheres polystyrene beads (580/605) (Invitrogen) were added to each well and incu-bated for 30 minutes with gentle shaking. To harvest the cells, the wells were washed with PBS, and 0.5 mL of 0.25% trypsin-EDTA (Gibco) was added for 5 minutes. For flow cytometric analysis, the harvested cells were washed with FACS buffer and blocked with Fc Block (BD) for 10 minutes at 4°C. Cell surface staining was performed in FACS buffer con-taining PerCP/Cy5.5-CD45 and fluorescein-5-isothiocyanate (FITC)-CD11b on ice for 1 hour. After washing with FACS buffer 3 times, the cells were analyzed using the BD LSR Fortessa cytometer. FluoSpheres polystyrene beads were detected according to PE fluorescence.

For analysis of stomach macrophage phagocytic activ-ity to *H pylori*–SS1, *Helicobacter felis*, *L monocytogenes*, and *S flexneri*, the bacteria were opsonized by incubating with normal murine serum for 60 minutes at 25°C with rotation and washed 3 times with PBS. Complement-opsonized bacteria then were labeled with 1 μmol/L of CFSE (65-0850-84; eBioscience) for 20 minutes at 25°C in the dark. CFSE-labeled bacteria were washed with PBS, centrifuged at 1700 × g for 10 minutes, and incubated with 100% FBS for 10 minutes at 37°C. CFSE-labeled bacteria were washed again, added to each well at 1×10^8 CFU per well, and incubated for 30 minutes in a 37°C, 5% CO$_2$ incubator. The subsequent steps were the same as described earlier for assessment of flow cytometric anal-ysis. For macrophage-receptor neutralization, the cells were pretreated with 1 μg/mL isotype-matched control IgG, anti-CD21/35 (7E9), or anti-VSIG4 (NLA14) for 30 minutes before infection.

Stomach Bacteria Quantification

The total stomach tissue was opened by cutting the greater curvature and the contents of the stomach were obtained without PBS washing. After the forestomach was discarded, the body and antrum tissues were cut into approximately 1-mm^3 pieces, and a one-fifth volume sam-ple was placed in 1.5-mL tubes containing 1 mL PBS and vortexed vigorously for 20 seconds. The sample was seri-ally diluted by transferring 100 μL to a new 900-μL PBS tube. To count the stomach bacteria CFU, 20 μL of the diluted sample was spotted 4–5 times on blood agar (Asan Pharmaceutical), Luria-Bertani agar (Sigma Aldrich), or brain heart infusion agar (BD) and incubated for 5 days at

37°C in an aerobic or anaerobic condition. For anaerobic incubation, agar plates were placed in the chamber in the presence of GasPak (BD).

Microbiota Depletion and Acidification

To generate microbiota-depleted FVB mice, the mice were supplied water containing an antibiotic cocktail (1 g/
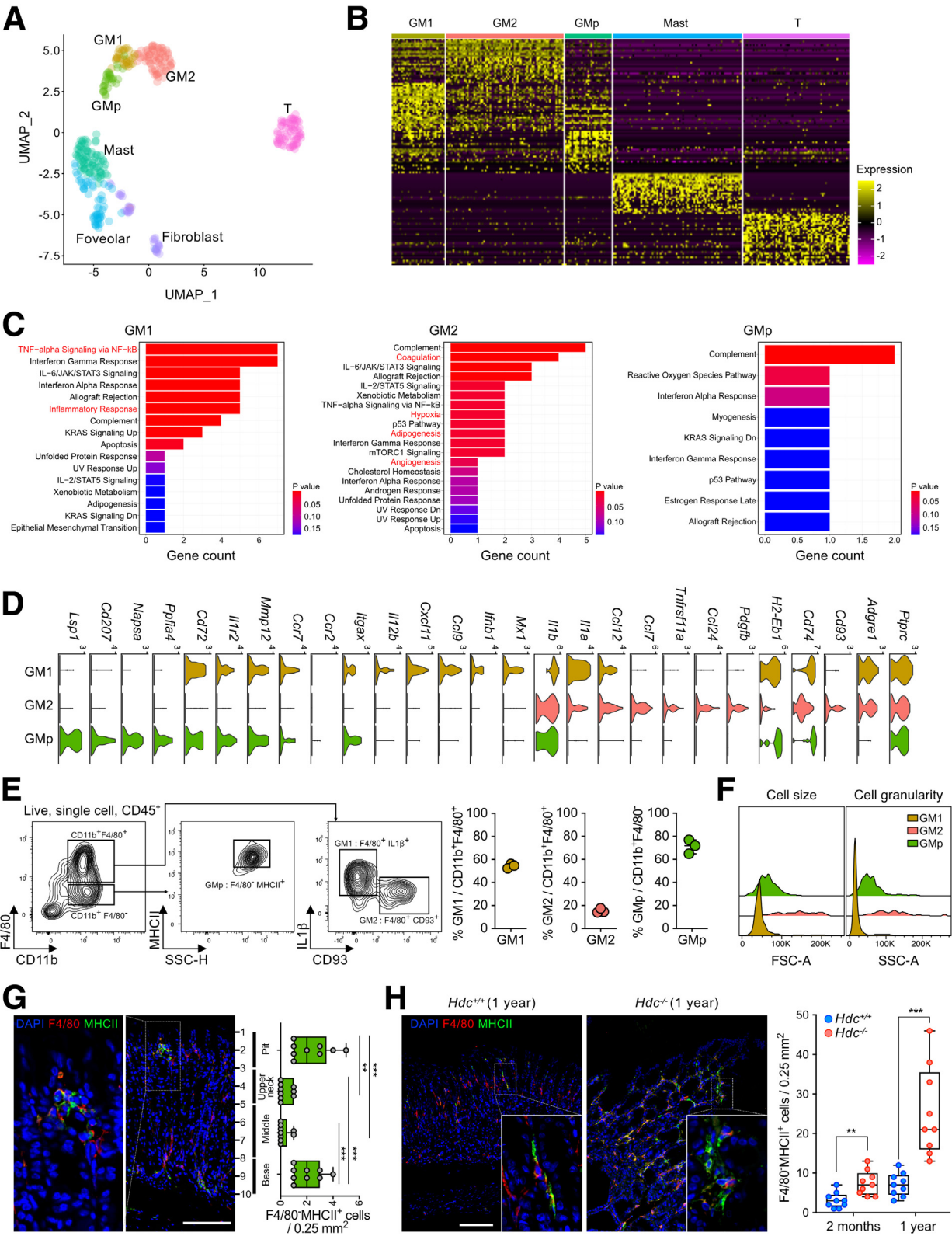
L ampicillin, 0.5 g/L vancomycin, 1 g/L metronidazole, 1 g/L neomycin, and 2.5 mg/L amphotericin B) for 7 days, which was withdrawn 24 hours before inoculation. At day −1, the mice were orally injected with the stomach microbiota obtained from a 4-week-old FVB mouse. The next day (day 0), HCl-treated water[26] was supplied for 30 days to create an acidified stomach environment. In brief, the water was acidified by adding 0.215 mL pure HCl (12N; Sigma) to 1 L water (pH 7) after autoclaving, and the pH was confirmed to be 2.6–2.8. The HCl-treated water was changed every other day. The stomach pH was determined at an average of 9 spots using Hydrion Brilliant pH dip sticks (Sigma).

Immunoblot Analysis

BM cells were pelleted and lysed in RIPA buffer (Sigma) with Halt Protease and Phosphatase Inhibitor Cocktail (Thermo) for 45 minutes on ice and then centrifuged at $16,100 \times g$ for 10 minutes at 4°C. Total proteins extracted from cells (40 μg) were run on a sodium dodecyl sulfate–polyacrylamide gel electrophoresis gel, transferred to polyvinylidene fluoride membranes (IPVH00010; Millipore), and developed with antibodies against phospho-ERK (Cell Signaling Technology), ERK (Cell Signaling Technology), phospho-p38 (Cell Signaling Technology), p38 (Cell Signaling Technology), phospho-JNK (Cell Signaling Technology), JNK (Cell Signaling Technology), and β-actin (Abcam). The bound antibodies then were reacted with horseradish peroxidase–linked anti-rabbit IgG or anti-mouse IgG secondary antibody and detected by SuperSignal West Femto Maximun Sensitivity Substrate (Thermo).

Generation of Chimeric Mice

Busulfan-conditioned BM transplantation was conducted according to the method of Ashizuka et al.[30] Busulfan (250 mg; Sigma) was dissolved in 1 mL dimethyl sulfoxide (Sigma), and 100 μL of the solution was mixed with 900 μL dimethyl sulfoxide and 4 mL prewarmed (37°C) PBS to create a 5 mg/mL solution. The age- and sex-matched 4-week-old male BM-recipient mice were weighed and 0.5 mg/20 g of busulfan was injected intraperitoneally 3 times every other day. Six days after the first busulfan injection, T-cell–depleted male BM

cells were prepared for transplantation. The tibias and femurs obtained from donor mice were flushed with Ca^{2+}/Mg^{2+}-free PBS (Sigma) using a 26G needle, and the BM cells were filtered through a 70-μm cell strainer (Falcon) into a 50-mL tube. The cells were centrifuged at $300 \times g$ for 5 minutes and resuspended in ice-cold magnetic-activated cell sorting (MACS) buffer (PBS, pH 7.2, 0.5% bovine serum albumin, 2 mmol/L EDTA). T cells were depleted using CD3ε microbeads (Miltenyi) according to the manufacturer's protocol. In brief, the cells were resuspended in 100 μL MACS buffer and labeled with 10 μL CD3ε-biotin antibody per 10^7 total BM cells for 10 minutes on ice. The cells were washed by centrifugation ($300 \times g$ for 10 min) and resuspended in 80 μL MACS buffer. Twenty microliters of antibiotin microbeads were added to the cells, incubated for 15 minutes on ice, washed, resuspended, and applied to the LD column (Miltenyi) to deplete CD3ε^+ T cells from total BM cells. T-cell–depleted BM cells were resuspended in PBS at 2×10^8 cells/mL and 200 μL of the suspension was delivered to the recipient mouse by intravenous injection to the tail vein. Busulfan-mediated specific cell depletion and BM transplant-mediated cell reconstitution were validated by flow cytometric analysis.

scRNA-seq

scRNA-seq libraries were prepared using 10× chromium Next GEM Single Cell 3' Library and Gel Bead Kit v3.1 (10x Genomics, Pleasanton, CA) and Chromium Single Cell Chip G (10x Genomics) according to the manufacturer's instructions. The cell suspensions were diluted in nuclease-free water to achieve a targeted cell count of 10,000. The cell suspension was mixed with Master Mix and loaded with Single Cell 3' v3.1 Gel Beads and partitioning oil into a chromium Next GEM Chip G system. RNA transcripts from single cells were uniquely barcoded and reverse-transcribed within droplets. cDNA molecules were pooled subject to an end-repair process, the addition of a single "A" base, followed by ligation of the adapters. The purified libraries were quantified using qPCR according to the Kapa Biosystems (London, UK)_qPCR Quantification protocol and qualified using the Agilent Technologies 4200 Tape Station (Agilent Technologies, Santa Clara, CA). The libraries were sequenced using the HiSeq platform (Illumina) according to the read length as instructed in the user guide.

Figure 10. (*See previous page*). **Single-cell transcriptome atlas of mouse stomach macrophages.** (*A*) Highlighted uniform manifold approximation and projection (UMAP) clustering of immune cells. (*B*) Heat map of differentially expressed genes for each cluster with an area under the receiver operating curve cut-off value ≥0.85. (*C*) Hallmark analysis of GM1, GM2, and GMp. M1- or M2-type gene signatures are highlighted in red. (*D*) Violin plots of the expression levels of representative macrophage marker genes. The y-axis shows the log scale–normalized read count. (*E and F*) Flow cytometry gating strategy to characterize GM1, GM2, and GMp macrophages. (*E*) Two-month-old mouse stomach cells were first gated on live (DAPI⁻), single cells, and CD45⁺ cells; CD45⁺ cells were distinguished by (1) CD11b⁺F4/80⁺ and further identified by IL1b⁺ or CD93⁺, and (2) CD11b⁺F4/80⁻ and further identified by MHCII⁺. (*F*) Comparison of forward scatter-area (FSC-A) and side scatter-area (SSC-A) levels between the GM1, GM2, and GMp macrophages (n = 3 mice). (*G and H*) Immunofluorescence (IF) staining of F4/80 (red), MHCII (green), and DAPI (blue) in the mouse stomach tissue. (*G*) To quantify F4/80⁻MHCII⁺ cells, 2-month-old *Hdc*⁻/⁻ stomach mucosal tissues were subdivided into 10 fractions (from the base to pit), and F4/80⁻MHCII⁺ cells were calculated for each region. (*H*) Representative IF images of the stomach fundus region in 1-year-old *Hdc*⁺/⁺ and *Hdc*⁻/⁻ mice, and quantification of F4/80⁻MHCII⁺ cells in a 0.24-mm² field. *Scale bar*: 100 μm. Data are shown as means ± SD. **$P < .01$, ***$P < .001$. DAPI, 4′,6-diamidino-2-phenylindole; Foveolar, foveolar cell; GM1, GM2, and GMp, stomach macrophages; JAK, janus kinase; KRAS, kirsten rat sarcoma viral oncogene homolog; Mast, mast cell; SSC-H, side scatter-height; STAT, signal transducer and activator of transcription; T, T cell; TNF, tumor necrosis factor.
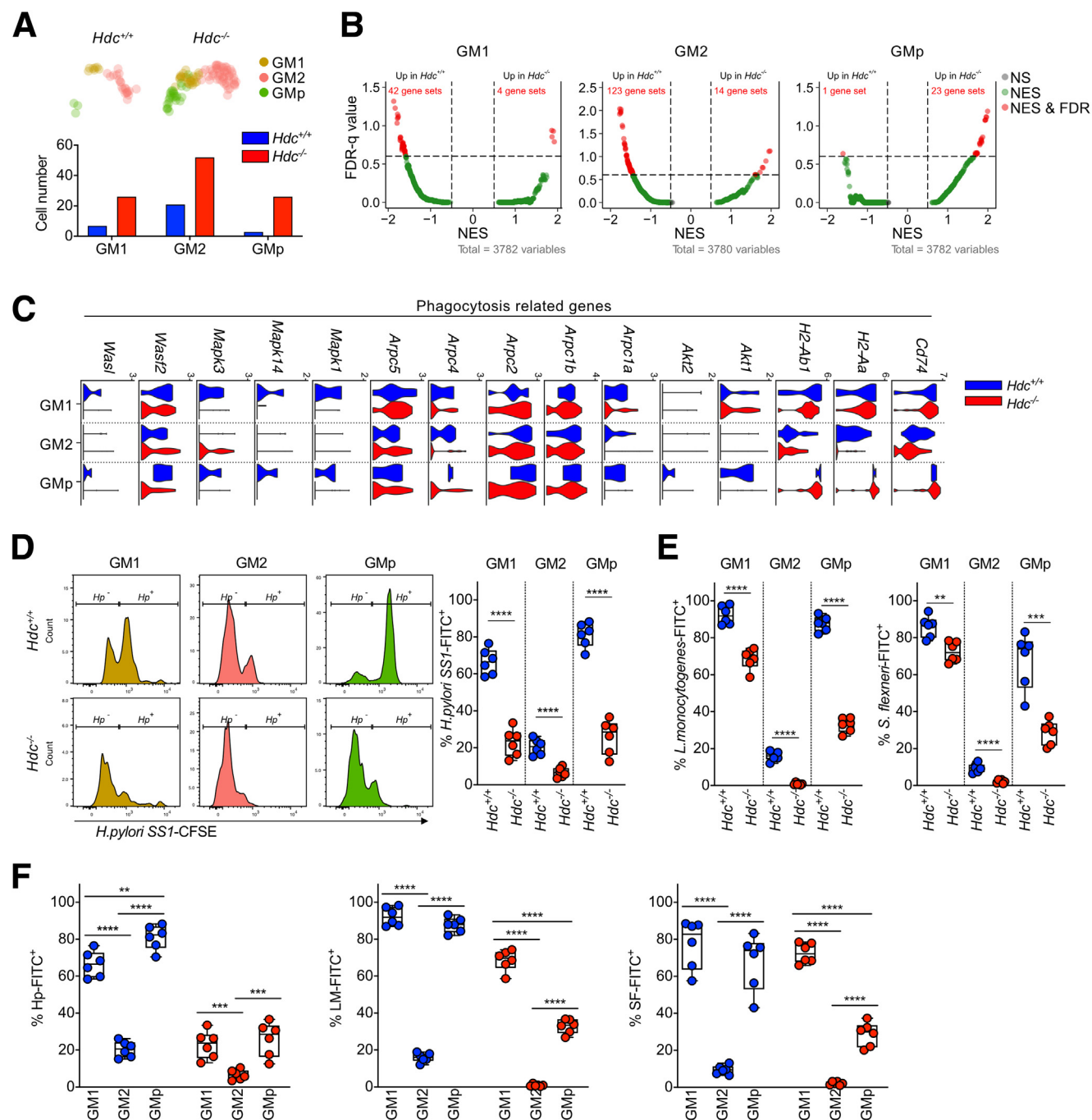
Figure 11. Molecular and functional comparison between $Hdc^{+/+}$ and $Hdc^{-/-}$ GMs. (A) Highlighted $Hdc^{+/+}$ and $Hdc^{-/-}$ GM clusters from Figure 9A, and determination of cell numbers in each cluster. (B) Scatter plots showing the differentially expressed gene sets between $Hdc^{+/+}$ and $Hdc^{-/-}$ GM clusters. (C) Violin plots of the expression levels of phagocytosis-related genes in GM clusters. (D) Phagocytosis assay of $Hdc^{+/+}$ and $Hdc^{-/-}$ stomach GM1, GM2, and GMp cells using CFSE-labeled H $pylori$–SS1. The percentage of CFSE-positive cells was calculated (n = 6 mice). (E) Phagocytosis assay of $Hdc^{+/+}$ and $Hdc^{-/-}$ stomach GM1, GM2, and GMp cells using CFSE-labeled L $monocytogenes$ or S $flexneri$. The percentage of CFSE-positive cells was calculated (n = 6 mice). (F) The phagocytic activities based on panels D and E of each macrophage population were compared. Data are presented as means ± SD. $**P < .01$, $***P < .001$, $****P < .0001$. FDR, false discovery rate; FITC, fluorescein-5-isothiocyanate; Hp, $Helicobacter$ $pylori$; LM, $Listeria$ $monocytogenesS$; NS, not significant; NES, normalized enrichment score; SF, $Shigella$ $flexneri$.
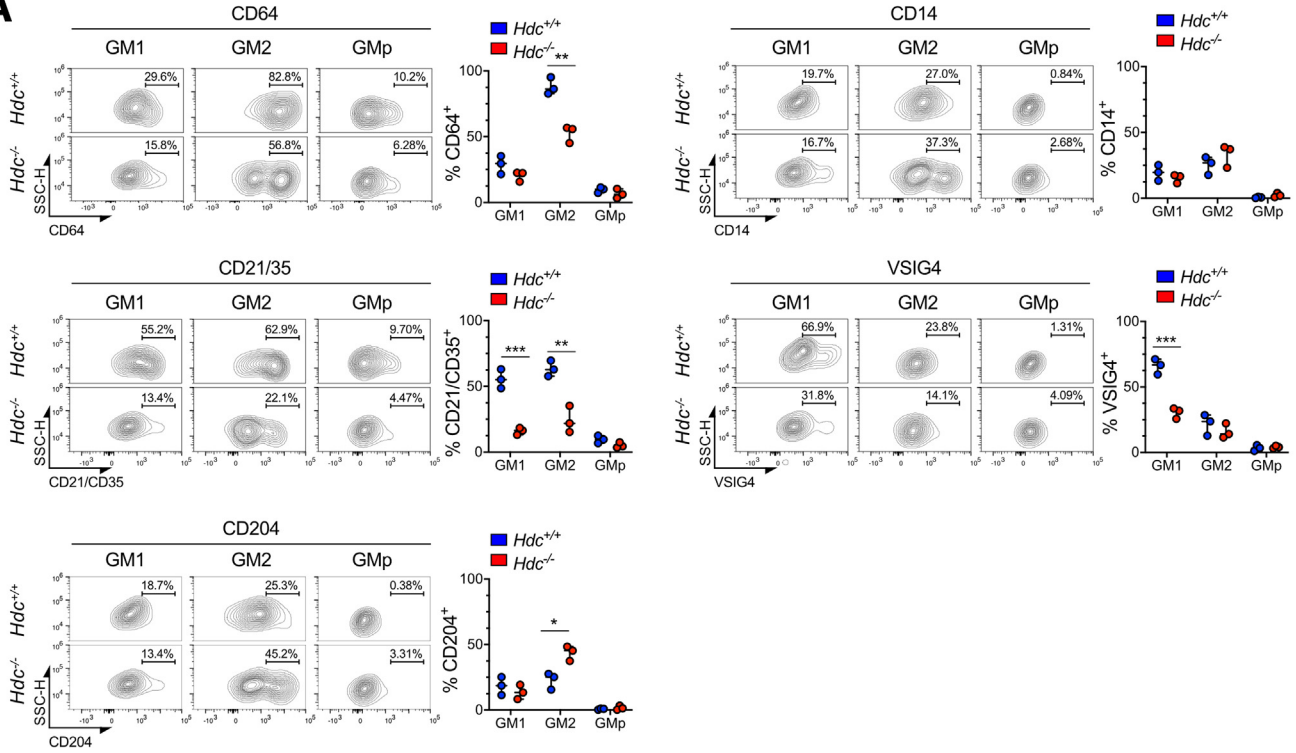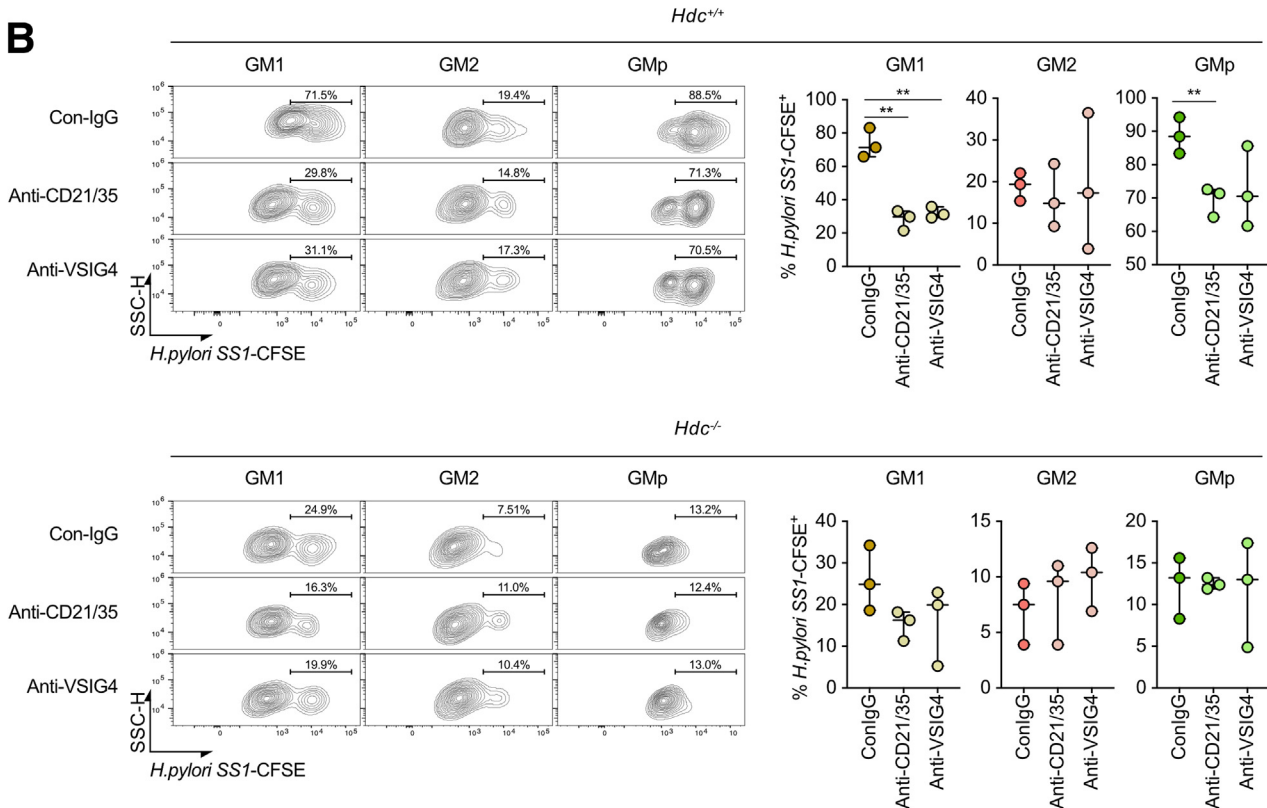
A

B

Figure 12. Impaired expression of phagocytosis-related receptors and receptor-mediated phagocytosis in stomach macrophages of *Hdc*$^{-/-}$ mice. (*A*) Expression of CD64, CD21/35, CD204, CD14, and VSIG4 was determined using flow cytometry on GM1, GM2, and GMp populations obtained from the stomach tissue of *Hdc*$^{+/+}$ and *Hdc*$^{-/-}$ mice. (*B*) Phagocytosis assay of control IgG (con-IgG)–, anti-CD21/35–, or anti-VSIG4–treated *Hdc*$^{+/+}$ and *Hdc*$^{-/-}$ stomach GM1, GM2, and GMp cells using CFSE-labeled *H felis.* The percentage of CFSE-positive cells was calculated (n = 3 mice). Data are presented as means ± SD. *P < .05, **P < .01, ***P < .001. SSC-H, side scatter-height.

Processing and Analysis of scRNA-seq Data

Cell Ranger (version 3.1.0, 10x Genomics) was used to process the raw data. The raw unique molecular identifier count matrix was converted into a Seurat object by the R package Seurat (version 3.2.3). The quality-control filtering of cells and genes was performed only using cells with at least 200 detected transcripts; cells with more than 30 mitochondrial DNA read counts were excluded. In addition, to eliminate potential doublets, single cells with more than 6000 genes detected were filtered out. Finally, 20,895 single cells remained, which were applied in downstream analyses using Seurat, following uniform manifold approximation and projection dimensional reduction. To remove batch effects, we used fastMNN, which detects mutual nearest neighbors of cells in different batches. After correcting for batch effects, the single cells were clustered using Find-Neighbors (using the 30 principal components for dimension reduction) and the FindClusters function (resolution = 2) in Seurat. Conventional markers were used to categorize every cell cluster into a known biological cell type. First, total cells were classified into 32 distinct clusters and similar clusters were merged based on the number of DEGs (>10). Next, the cells were classified into 13 clusters and 10 cell types were annotated based on conventional markers. The immune cell cluster (370 cells) was isolated from the total stomach cells and reclustered by Seurat; the immune cells were classified into 7 distinct clusters. The Seurat Findallmarkers function was executed to identify preferentially expressed genes in clusters or DEGs between $Hdc^{-/-}$ and wild-type cells. Heatmaps were generated by the DoHeatmap function in the Seurat package. GSEA was conducted using the EnrichR package (version 3.0), selecting the top 18 genes from each cell type for the HALLMARK analysis. Pathway analyses were performed with GSEA (https://www.gsea-msigdb.org/gsea/index.jsp), and the results were visualized by volcano plots generated using the EnhancedVolcano package (version 1.4.0). Raw sequencing data have been submitted to Korean Nucleotide Archive (KoNA) database repository (KRA2100216).

Quantification and Statistical Analysis

Statistical analyses were performed with Prism software (GraphPad). To evaluate statistical significance, differences between groups were compared with the Student t test. A P value less than .05 was considered statistically significant. Statistical details, including sample sizes, for each experiment are provided in the relevant figure legends.

References

1. Joseph DR, Sullivan PM, Wang YM, Kozak C, Fenstermacher DA, Behrendsen ME, Zahnow CA. Characterization and expression of the complementary DNA encoding rat histidine decarboxylase. Proc Natl Acad Sci U S A 1990;87:733–737.
2. Higuchi S, Tanimoto A, Arima N, Xu H, Murata Y, Hamada T, Makishima K, Sasaguri Y. Effects of histamine and interleukin-4 synthesized in arterial intima on phagocytosis by monocytes/macrophages in relation to atherosclerosis. FEBS Lett 2001;505:217–222.
3. Zwadlo-Klarwasser G, Vogts M, Hamann W, Belke K, Baron J, Schmutzler W. Generation and subcellular distribution of histamine in human blood monocytes and monocyte subsets. Inflamm Res 1998;47:434–439.
4. Nakamura E, Kataoka T, Furutani K, Jimbo K, Aihara T, Tanaka S, Ichikawa A, Ohtsu H, Okabe S. Lack of histamine alters gastric mucosal morphology: comparison of histidine decarboxylase-deficient and mast cell-deficient mice. Am J Physiol Gastrointest Liver Physiol 2004;287:G1053–G1061.
5. Nozaki K, Weis V, Wang TC, Falus A, Goldenring JR. Altered gastric chief cell lineage differentiation in histamine-deficient mice. Am J Physiol Gastrointest Liver Physiol 2009;296:G1211–G1220.
6. Yang XD, Ai W, Asfaha S, Bhagat G, Friedman RA, Jin G, Park H, Shykind B, Diacovo TG, Falus A, Wang TC. Histamine deficiency promotes inflammation-associated carcinogenesis through reduced myeloid maturation and accumulation of CD11b+Ly6G+ immature myeloid cells. Nat Med 2011;17:87–95.
7. Ahn B, Kohanbash G, Ohkuri T, Kosaka A, Chen X, Ikeura M, Wang TC, Okada H. Histamine deficiency promotes accumulation of immunosuppressive immature myeloid cells and growth of murine gliomas. Oncoimmunology 2015;4:e1047581.
8. Xu L, Cheng D, Huang Z, Ding S, Zhang W, Tan H, Shi H, Chen R, Zou Y, Wang TC, Yang X, Ge J. Histamine promotes the differentiation of macrophages from CD11b(+) myeloid cells and formation of foam cells through a Stat6-dependent pathway. Atherosclerosis 2017;263:42–52.
9. Abudupataer M, Zou W, Zhang W, Ding S, Zhou Z, Chen J, Li H, Zhang Z, Wang C, Ge J, Hong T, Yang X. Histamine deficiency delays ischaemic skeletal muscle regeneration via inducing aberrant inflammatory responses and repressing myoblast proliferation. J Cell Mol Med 2019;23:8392–8409.
10. Martner A, Wiktorin HG, Lenox B, Ewald Sander F, Aydin E, Aurelius J, Thoren FB, Stahlberg A, Hermodsson S, Hellstrand K. Histamine promotes the development of monocyte-derived dendritic cells and reduces tumor growth by targeting the myeloid NADPH oxidase. J Immunol 2015;194:5014–5021.
11. Chen X, Deng H, Churchill MJ, Luchsinger LL, Du X, Chu TH, Friedman RA, Middelhoff M, Ding H, Tailor YH, Wang ALE, Liu H, Niu Z, Wang H, Jiang Z, Renders S, Ho SH, Shah SV, Tishchenko P, Chang W, Swayne TC, Munteanu L, Califano A, Takahashi R, Nagar KK, Renz BW, Worthley DL, Westphalen CB, Hayakawa Y, Asfaha S, Borot F, Lin CS, Snoeck HW, Mukherjee S, Wang TC. Bone marrow myeloid cells regulate myeloid-biased hematopoietic stem cells via a histamine-dependent feedback loop. Cell Stem Cell 2017; 21:747–760 e7.
12. Mommert S, Ratz L, Stark H, Gutzmer R, Werfel T. The histamine H4 receptor modulates the differentiation process of human monocyte-derived M1 macrophages and the release of CCL4/MIP-1beta from fully differentiated M1 macrophages. Inflamm Res 2018;67:503–513.

13. Gordon S. The macrophage: past, present and future. Eur J Immunol 2007;37(Suppl 1):S9–S17.

14. Mantovani A, Biswas SK, Galdiero MR, Sica A, Locati M. Macrophage plasticity and polarization in tissue repair and remodelling. J Pathol 2013;229:176–185.

15. Wang J, Chen WD, Wang YD. The relationship between gut microbiota and inflammatory diseases: the role of macrophages. Front Microbiol 2020;11:1065.

16. Zavros Y, Rieder G, Ferguson A, Samuelson LC, Merchant JL. Genetic or chemical hypochlorhydria is associated with inflammation that modulates parietal and G-cell populations in mice. Gastroenterology 2002; 122:119–133.

17. Ogawa T, Maeda K, Tonai S, Kobayashi T, Watanabe T, Okabe S. Utilization of knockout mice to examine the potential role of gastric histamine H2-receptors in Menetrier's disease. J Pharmacol Sci 2003;91:61–70.

18. Matsuo J, Kimura S, Yamamura A, Koh CP, Hossain MZ, Heng DL, Kohu K, Voon DC, Hiai H, Unno M, So JB, Zhu F, Srivastava S, Teh M, Yeoh KG, Osato M, Ito Y. Identification of stem cells in the epithelium of the stomach corpus and antrum of mice. Gastroenterology 2017;152:218–231 e14.

19. Weis VG, Petersen CP, Weis JA, Meyer AR, Choi E, Mills JC, Goldenring JR. Maturity and age influence chief cell ability to transdifferentiate into metaplasia. Am J Physiol Gastrointest Liver Physiol 2017;312:G67–G76.

20. Hirata K, Suzuki H, Imaeda H, Matsuzaki J, Tsugawa H, Nagano O, Asakura K, Saya H, Hibi T. CD44 variant 9 expression in primary early gastric cancer as a predictive marker for recurrence. Br J Cancer 2013;109:379–386.

21. Newman AM, Liu CL, Green MR, Gentles AJ, Feng W, Xu Y, Hoang CD, Diehn M, Alizadeh AA. Robust enumeration of cell subsets from tissue expression profiles. Nat Methods 2015;12:453–457.

22. Petersen CP, Meyer AR, De Salvo C, Choi E, Schlegel C, Petersen A, Engevik AC, Prasad N, Levy SE, Peebles RS, Pizarro TT, Goldenring JR. A signalling cascade of IL-33 to IL-13 regulates metaplasia in the mouse stomach. Gut 2018;67:805–817.

23. Czerner CP, Klos A, Seifert R, Neumann D. Histamine induces chemotaxis and phagocytosis in murine bone marrow-derived macrophages and RAW 264.7 macrophage-like cells via histamine H4-receptor. Inflamm Res 2014;63:239–247.

24. Mowat AM, Scott CL, Bain CC. Barrier-tissue macrophages: functional adaptation to environmental challenges. Nat Med 2017;23:1258–1270.

25. Lindstrom E, Chen D, Norlen P, Andersson K, Hakanson R. Control of gastric acid secretion: the gastrin-ECL cell-parietal cell axis. Comp Biochem Physiol A Mol Integr Physiol 2001;128:505–514.

26. Calvete O, Varro A, Pritchard DM, Barroso A, Oteo M, Morcillo MA, Vargiu P, Dodd S, Garcia M, Reyes J, Ortega S, Benitez J. A knockin mouse model for human ATP4aR703C mutation identified in familial gastric neuroendocrine tumors recapitulates the premalignant condition of the human disease and suggests new therapeutic strategies. Dis Model Mech 2016; 9:975–984.

27. Ellenbogen L, Kelly RG, Taylor RJ Jr, Stubbs CS Jr. Studies on the inhibition of histidine decarboxylase, aromatic-L-amino acid decarboxylase and acid secretion by brocresine and its metabolites. Biochem Pharmacol 1973;22:939–947.

28. Richardson ET, Shukla S, Nagy N, Boom WH, Beck RC, Zhou L, Landreth GE, Harding CV. ERK signaling is essential for macrophage development. PLoS One 2015; 10:e0140064.

29. Mosser DM, Edwards JP. Exploring the full spectrum of macrophage activation. Nat Rev Immunol 2008; 8:958–969.

30. Ashizuka S, Peranteau WH, Hayashi S, Flake AW. Busulfan-conditioned bone marrow transplantation results in high-level allogeneic chimerism in mice made tolerant by in utero hematopoietic cell transplantation. Exp Hematol 2006;34:359–368.

31. Lantz C, Radmanesh B, Liu E, Thorp EB, Lin J. Single-cell RNA sequencing uncovers heterogenous transcriptional signatures in macrophages during efferocytosis. Sci Rep 2020;10:14333.

32. Polk DB, Peek RM Jr. Helicobacter pylori: gastric cancer and beyond. Nat Rev Cancer 2010;10:403–414.

33. Gray ML, Killinger AH. Listeria monocytogenes and listeric infections. Bacteriol Rev 1966;30:309–382.

34. Zychlinsky A, Prevost MC, Sansonetti PJ. Shigella flexneri induces apoptosis in infected macrophages. Nature 1992;358:167–169.

35. Freeman SA, Grinstein S. Phagocytosis: receptors, signal integration, and the cytoskeleton. Immunol Rev 2014;262:193–215.

36. Indik ZK, Hunter S, Huang MM, Pan XQ, Chien P, Kelly C, Levinson AI, Kimberly RP, Schreiber AD. The high affinity Fc gamma receptor (CD64) induces phagocytosis in the absence of its cytoplasmic domain: the gamma subunit of Fc gamma RIIIA imparts phagocytic function to Fc gamma RI. Exp Hematol 1994;22:599–606.

37. Kane SJ, Swanson E, Gordon EO, Rocha S, Bender HR, Donius LR, Aguzzi A, Hannan JP, Zabel MD. Relative impact of complement receptors CD21/35 (Cr2/1) on scrapie pathogenesis in mice. mSphere 2017;2:e00493.

38. Todt JC, Hu B, Curtis JL. The scavenger receptor SR-A I/II (CD204) signals via the receptor tyrosine kinase Mertk during apoptotic cell uptake by murine macrophages. J Leukoc Biol 2008;84:510–518.

39. Zanoni I, Ostuni R, Marek LR, Barresi S, Barbalat R, Barton GM, Granucci F, Kagan JC. CD14 controls the LPS-induced endocytosis of Toll-like receptor 4. Cell 2011;147:868–880.

40. Kim KH, Choi BK, Kim YH, Han C, Oh HS, Lee DG, Kwon BS. Extracellular stimulation of VSIG4/complement receptor Ig suppresses intracellular bacterial infection by inducing autophagy. Autophagy 2016;12:1647–1659.

41. Martinez FO, Helming L, Gordon S. Alternative activation of macrophages: an immunologic functional perspective. Annu Rev Immunol 2009;27:451–483.

42. Cassado Ados A, D'Imperio Lima MR, Bortoluci KR. Revisiting mouse peritoneal macrophages: heterogeneity, development, and function. Front Immunol 2015; 6:225.

43. Scott DR, Weeks D, Hong C, Postius S, Melchers K, Sachs G. The role of internal urease in acid resistance of Helicobacter pylori. Gastroenterology 1998;114:58–70.

44. Watari J, Chen N, Amenta PS, Fukui H, Oshima T, Tomita T, Miwa H, Lim KJ, Das KM. Helicobacter pylori associated chronic gastritis, clinical syndromes, precancerous lesions, and pathogenesis of gastric cancer development. World J Gastroenterol 2014;20:5461–5473.

45. Parsonnet J, Friedman GD, Vandersteen DP, Chang Y, Vogelman JH, Orentreich N, Sibley RK. Helicobacter pylori infection and the risk of gastric carcinoma. N Engl J Med 1991;325:1127–1131.

46. Klausz G, Buzas E, Scharek P, Tiszlavicz L, Gyulai Z, Fulop AK, Falus A, Mandi Y. Effects of Helicobacter pylori infection on gastric inflammation and local cytokine production in histamine-deficient (histidine decarboxylase knock-out) mice. Immunol Lett 2004; 94:223–228.

47. Perez-Munoz ME, Arrieta MC, Ramer-Tait AE, Walter J. A critical assessment of the "sterile womb" and "in utero colonization" hypotheses: implications for research on the pioneer infant microbiome. Microbiome 2017;5:48.

48. Smith K, McCoy KD, Macpherson AJ. Use of axenic animals in studying the adaptation of mammals to their commensal intestinal microbiota. Semin Immunol 2007; 19:59–69.

49. Carvalho BS, Irizarry RA. A framework for oligonucleotide microarray preprocessing. Bioinformatics 2010; 26:2363–2367.

50. Martignetti L, Calzone L, Bonnet E, Barillot E, Zinovyev A. ROMA: representation and quantification of module activity from target expression data. Front Genet 2016;7:18.

51. Liberzon A, Subramanian A, Pinchback R, Thorvaldsdottir H, Tamayo P, Mesirov JP. Molecular signatures database (MSigDB) 3.0. Bioinformatics 2011; 27:1739–1740.

52. Chen Z, Huang A, Sun J, Jiang T, Qin FX, Wu A. Inference of immune cell composition on the expression profiles of mouse tissue. Sci Rep 2017;7:40508.

53. Herlemann DP, Labrenz M, Jurgens K, Bertilsson S, Waniek JJ, Andersson AF. Transitions in bacterial communities along the 2000 km salinity gradient of the Baltic Sea. ISME J 2011;5:1571–1579.

54. Magoc T, Salzberg SL. FLASH: fast length adjustment of short reads to improve genome assemblies. Bioinformatics 2011;27:2957–2963.

55. Li W, Fu L, Niu B, Wu S, Wooley J. Ultrafast clustering algorithms for metagenomic sequence analysis. Brief Bioinform 2012;13:656–668.

56. Zhang Z, Schwartz S, Wagner L, Miller W. A greedy algorithm for aligning DNA sequences. J Comput Biol 2000;7:203–214.

Correspondence
Kyung-Min Lim, PhD, College of Pharmacy, Ewha Womans University, Seoul 03760, Republic of Korea. e-mail: kmlim@ewha.ac.kr; or Ki Taek Nam, DVM, PhD, Severance Biomedical Science Institute, Brain Korea 21 PLUS Project for Medical Science, Yonsei University College of Medicine, Seoul 03722, Republic of Korea. e-mail: KITAEK@yuhs.ac.